Behavioral Strategy Determines Frontal or Posterior Location of Short-Term Memory in Neocortex

Gilad, Ariel ; Gallero-Salas, Yasir ; Groos, Dominik ; Helmchen, Fritjof

Abstract: The location of short-term memory in mammalian neocortex remains elusive. Here we show that distinct neocortical areas maintain short-term memory depending on behavioral strategy. Using wide-field and single-cell calcium imaging, we measured layer 2/3 neuronal activity in mice performing a whisker-based texture discrimination task with delayed response. Mice either deployed an active strategy-engaging their body toward the approaching texture-or passively awaited the touch. Independent of strategy, whisker-related posterior areas encoded choice early after touch. During the delay, in contrast, persistent cortical activity was located medio-frontally in active trials but in a lateral posterior area in passive trials. Perturbing these areas impaired performance for the associated strategy and also provoked strategy switches. Frontally maintained information related to future action, whereas activity in the posterior cortex reflected past stimulus identity. Thus, depending on behavioral strategy, cortical activity is routed differentially to hold information either frontally or posteriorly before converging to similar action. This project has received funding from the European Union's Horizon 2020 research and innovation programme under the Marie Skłodowska-Curie grant agreement No 659719

DOI: https://doi.org/10.1016/j.neuron.2018.07.029

Published in Neuron
Volume 99, Issue 4, 22 August 2018, Pages 814-828.e7
DOI: 10.1016/j.neuron.2018.07.029

Behavioral strategy determines frontal or posterior location of short-term memory in neocortex

Authors:
Ariel Gilad[1], Yasir Gallero-Salas[1,2], Dominik Groos[1,2] and Fritjof Helmchen[1,2]*

Affiliations:
[1] Brain Research Institute, University of Zurich, Zurich CH-8057, Switzerland.
[2] Neuroscience Center Zurich, Zurich CH-8057, Switzerland.

*Correspondence to lead contact: helmchen@hifo.uzh.ch

SUMMARY

Location of short-term memory in mammalian neocortex remains elusive. Here we show that distinct neocortical areas maintain short-term memory depending on behavioral strategy. Using wide-field and single-cell calcium imaging we measured layer 2/3 neuronal activity in mice performing a whisker-based texture discrimination task with delayed response. Mice either deployed an active strategy—engaging their body towards the approaching texture—or passively awaited the touch. Independent of strategy, whisker-related posterior areas encoded choice early after touch. During the delay, in contrast, persistent cortical activity was located medio-frontally in active trials but in a lateral posterior area in passive trials. Perturbing these areas impaired performance for the associated strategy and also provoked strategy switches. Frontally maintained information related to future action whereas activity in posterior cortex reflected past stimulus identity. Thus, depending on behavioral strategy cortical activity is routed differentially to hold information either frontally or posteriorly before converging to similar action.

INTRODUCTION

The mammalian brain integrates behaviorally relevant sensory information by recruiting large parts of the neocortex to enable precise perception, apt decisions and appropriate actions. However, we still poorly understand which neocortical regions are activated during specific behaviors and how they relate to behavioral parameters. Previous work showed that sensory information is represented and processed mainly in the posterior sensory cortices (Goard et al., 2016; Guo et al., 2014; Kwon et al., 2016; Miyashita and Feldman, 2013; Poort et al., 2015; Zhang et al., 2014), whereas action planning and preparation of movement execution are encoded in frontal motor cortices (Chen et al., 2017; Churchland et al., 2012; Erlich et al., 2011; Goard et al., 2016; Guo et al., 2014; Kiritani et al., 2016; Makino et al., 2017). In well-trained animals posterior sensory areas may also contain choice-related information early after initial sensation (Gilad et al., 2013; Harvey et al., 2012; Roelfsema et al., 2007; Yang et al., 2015).

It is less clear, where information is maintained in the intermediate phase of sensorimotor processing, i.e. between sensation and action. Specifically, it is still debated whether information relevant for guiding future actions is held in memory in frontal areas such as premotor cortices (Goard et al., 2016; Guo et al., 2014; Leavitt et al., 2017; Li et al., 2015; Romo and de Lafuente, 2013) or in posterior areas such as posterior parietal cortex (Harvey et al., 2012; Leavitt et al., 2017; Marcos and Harvey, 2016; Siegel et al., 2015). A key factor that could contribute to different cortical activity patterns is that subjects, specifically mice, can solve a complex task by deploying a variety of behavioral strategies (Diamond et al., 2008; Maravall and Diamond, 2015; Platt and Huettel, 2008; Venkatraman et al., 2009). For example, when a behaviorally relevant texture approaches the whiskers of mice, they tend to either actively seek the texture (‘active’ strategy or ‘generative’ mode; Guo et al., 2014; Knutsen et al., 2006; Maravall and Diamond, 2015; Morita et al., 2011) or, in

contrast, passively wait for the texture to touch their whiskers ('passive' strategy or 'receptive' mode; Maravall and Diamond, 2015; Miyashita and Feldman, 2013; Morita et al., 2011; Stüttgen and Schwarz, 2008). Given such behavioral variation in solving a particular task, the underlying cortical activity patterns for each strategy may greatly differ, not only for the stimulus-evoked response but possibly also during short-term memory when stimulus presentation is over. Here, we address this question by employing wide-field calcium imaging across mouse cortex, which has been applied previously to reveal activity patterns under anesthesia or resting state conditions (Ferezou et al., 2007; Mohajerani et al., 2013) but only recently during behavioral tasks (Allen et al., 2017; Chen et al., 2017; Makino et al., 2017). We find that mice deploy different behavioral strategies that are associated with highly distinct locations of cortical activity during short-term memory.

RESULTS

We trained transgenic GCaMP6f mice in a head-fixed go/no-go texture discrimination task (Chen et al., 2013), which we modified to include a short-term memory period by enforcing a delayed response (Figure 1A; STAR Methods). In each trial, after an initial auditory tone, a sandpaper panel with either coarse or smooth surface texture (grit sizes P100 and P1200, respectively) approached and touched the facial whiskers of the mouse. The texture stayed in place for a 'sensation period' of 2 seconds before it was withdrawn. In a subsequent 'delay period' the mouse had to hold information in short-term memory until another auditory cue signaled that it was allowed to respond by licking for a water reward. Using operant conditionng we trained 5 mice to lick for the P100 texture and 3 mice to lick for the P1200 texture. The water spout with licking detector always remained within reach at a fixed position. If the mouse licked too early, i.e., before the response cue, the trial was aborted and the mouse was mildly punished with an auditory white noise.

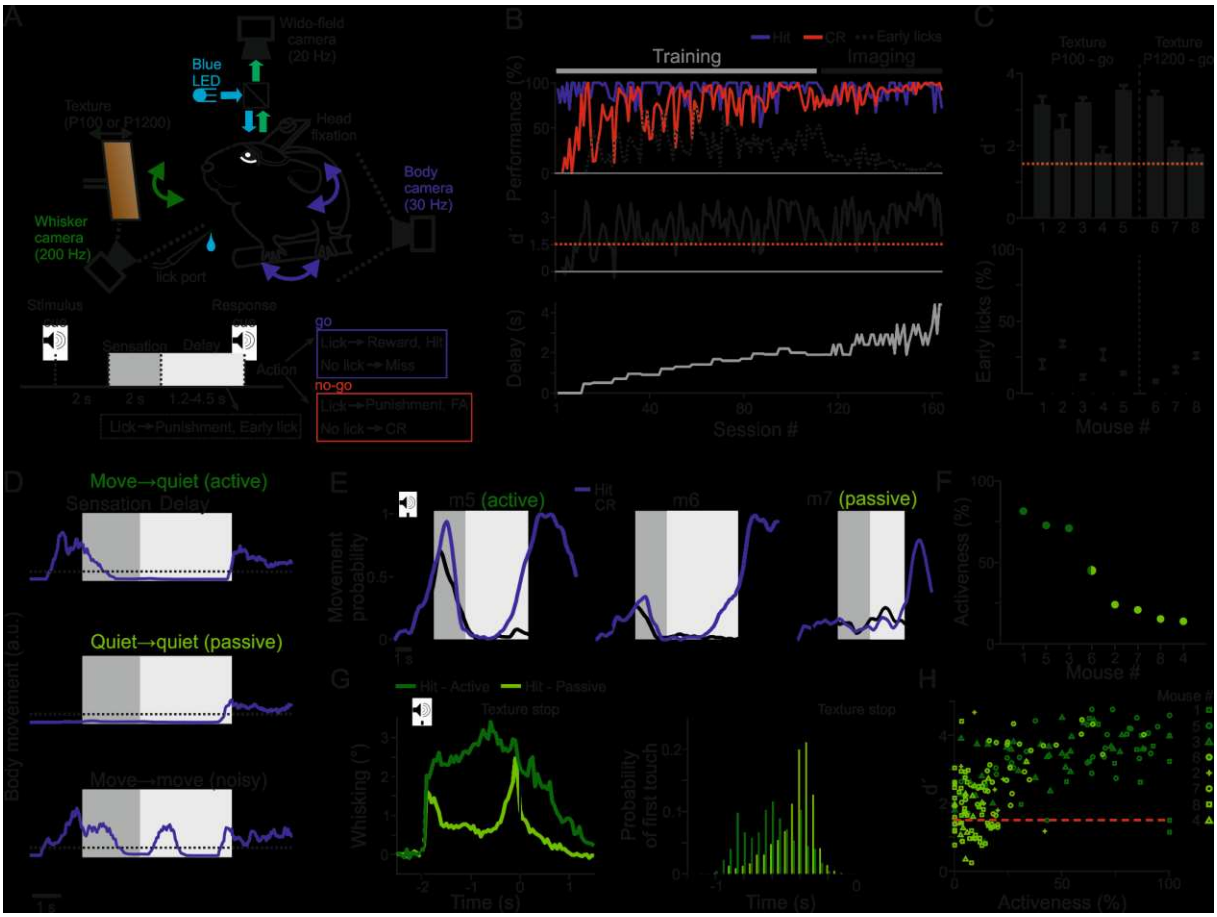

Figure 1. Mice can perform a texture discrimination task with delay using either an active or passive strategy.

(A) Top: Setup for head-fixed texture discrimination with a delay period and simultaneous wide-field calcium imaging and video monitoring of whisker motion and body movements. Bottom: Trial structure and possible trial outcomes.

(B) Performance and delay duration throughout training and imaging of one example mouse (mouse #6).

(C) Performance (d' and fraction of early lick trials) for each mouse. Error bars are s.e.m. over imaging sessions.

(D) Body movement during three example trials from one imaging session (high values depict movement; STAR Methods). Dashed black line indicates threshold to construct the corresponding binary movement vectors (lower black traces). Classification into active (dark green) and passive (light green) trials is based on movement during the sensation period. Trials with the mouse moving during the first second in the delay period were defined as noisy and discarded (bottom trial).

(E) Probability of movement across all hit and CR trials for three example mice (n = 39/51, 66/54 and 43/38 hit/CR trials for mouse #5, 6, and 7, respectively). Note differences in movement profiles across mice.

(F) Activeness for each mouse arranged in descending order.

(G) Examples from mouse #6 of whisking envelope as the texture approaches (left) and histogram of the times of first whisker-texture touch (right) for the different types of hit trials (active: dark green; passive: light green).

(H) Performance (d') as a function of activeness for each imaging session across mice.

See also Figure S1

During training, an increasing delay was gradually introduced over weeks (Figure 1B; training time 6.9 ± 0.3 weeks; mean ± s.e.m.; n = 8 mice). Mice learned to withhold licking for up to several seconds (range of 1.2-4.5 s). Although varying in their performance, all mice reached stable expert level (threshold of d' > 1.5) with a relatively low rate of early licks (Figure 1C; Figure S1A-C; STAR Methods). Once expert level was reached, we commenced wide-field calcium imaging of task-related neocortical activity with concurrent video monitoring of whisking and body movements (Figure 1A, B; n = 17, 8, 38, 16, 31, 24, 17, and 46 imaging sessions for mouse #1 to #8, respectively; STAR Methods).

Active versus passive strategy during texture discrimination

Mice displayed variable body movements throughout trials, pointing to different behavioral strategies (Figure 1D). In some hit trials mice strongly moved their body during the sensation period; they actively engaged the approaching texture, e.g., by moving their forelimbs along the support pole and arching their backs, but then remained quiet during most of the delay period (only starting to move again towards the end in preparation of the licking action). These trials we classified as 'active' trials. In other hit trials, even in the same session, mice instead stayed quiet throughout the sensation period (with the sandpaper still touching the whiskers) and most of the delay period; these trials were classified as 'passive' trials. Movement probability varied across mice, with some animals employing mostly the active strategy, others the passive strategy, and yet others alternating between strategies (Figure 1E; Figure S1B; STAR Methods). Use of strategies also varied within and across imaging days (Figure S1C; Discussion). 'Activeness', quantified as the percentage of hit trials with body movements prior and during the texture touch, varied across mice between 16 and 82% (Figure 1F; STAR Methods).

Is activeness linked to whisking activity and task performance? Mice whisked more towards the approaching texture in active versus passive trials, which also resulted in earlier first touches in active trials (Figure 1G; mean whisking envelope from -1 to +1 seconds relative to texture stop: 2.89° ± 0.36° vs. 0.95° ± 0.14°; $P < 0.05$; first touch time before texture stop: -0.52 ± 0.03 s vs. -0.42 ± 0.02 s; $P < 0.05$; n = 8 mice; Wilcoxon signed-rank test). In addition, d' performance positively correlated with activeness (Figure 1H; r = 0.6; $P < 0.001$) and passive mice were slower to reach expert level compared to active mice (Figure S1A; approximately 60 and 110 sessions for active and passive mice, respectively). Together these results suggest that in general the active strategy can be helpful for the mouse, albeit in many sessions mice also performed at high level (d' > 2.5) using the passive strategy. To further check the relationship between activeness and motivation, we calculated performance and activeness separately for the first and last 100 trials on each imaging day. Although in some cases performance and activeness decreased together at the end of the day—possibly indicating reduced motivation—on most imaging days (30 out of 50) activeness stayed at a similar level throughout the day (<10% reduction; Figure S1D, E). Specifically, we observed passive behavior at the beginning of the day and high activeness at the end of the day and overall the change in performance during the day was not significantly correlated with the change in activeness (r = 0.19; $P > 0.05$). These results are consistent with activeness being an integral part of a behavioral strategy to solve the task rather than purely reflecting motivation. We conclude that mice can solve the texture discrimination task using different behavioral strategies (active or passive), which raises the question whether these strategies are associated with distinct patterns of brain activity.

Sensory-related areas encode choice during sensation

To measure large-scale neocortical activity during behavior we applied wide-field calcium imaging through an intact skull preparation (Vanni and Murphy, 2014) in these transgenic

mice that expressed GCaMP6f in layer 2/3 (L2/3) excitatory neurons (Figure 2A; STAR Methods). For each mouse we mapped the activity patterns evoked by different sensory stimuli under anesthesia, allowing us to localize several neocortical areas including barrel cortex in primary somatosensory cortex (S1BC), secondary somatosensory cortex (S2), and rostrolateral posterior parietal cortex (RL), situated between S1BC and primary visual cortex (Figure 2A, B; Figure S2A; STAR Methods; Wang and Burkhalter, 2007; Wang et al., 2012).

We first examined spatiotemporal activity patterns in these sensory-related areas (S1BC, S2, and RL) during sensation. We created activity maps for a time window during texture touch ('sensation maps') and extracted the time course of GCaMP6f fluorescence changes ($\Delta F/F$) for regions of interests during the initial second after first touch (STAR Methods). All three areas displayed significantly enhanced activity during hit versus CR trials independent of texture type (Figure 2B, C; Figure S2B, C; for either P100 or P1200 as 'go' texture; $P < 0.05$; Wilcoxon signed-rank test for each mouse separately) as well as averaged across mice (Figure 2D; $P < 0.01$; Wilcoxon signed-rank test). Calcium signals peaked around 0.5 s after a first whisker touched the texture, presumably because it takes several hundreds of milliseconds for other whiskers to engage the texture and evoke the population signal that most likely represents responses to multiple whisker contacts. Discrimination between hit and CR trials occurred within a few hundred milliseconds, in line with previous studies (Chen et al., 2013, 2016). In control experiments we excluded confounding effects of autofluorescence or non-calcium-related intrinsic signals (STAR Methods and Figure S3). In addition, we trained three extra transgenic mice in a similar delay task without texture discrimination (i.e., both textures resulted in a reward when licking after a delay period; STAR Methods). These mice showed no significant difference of evoked fluorescence changes in S1BC, S2, and RL between the P100 and P1200 textures (Figure S4).

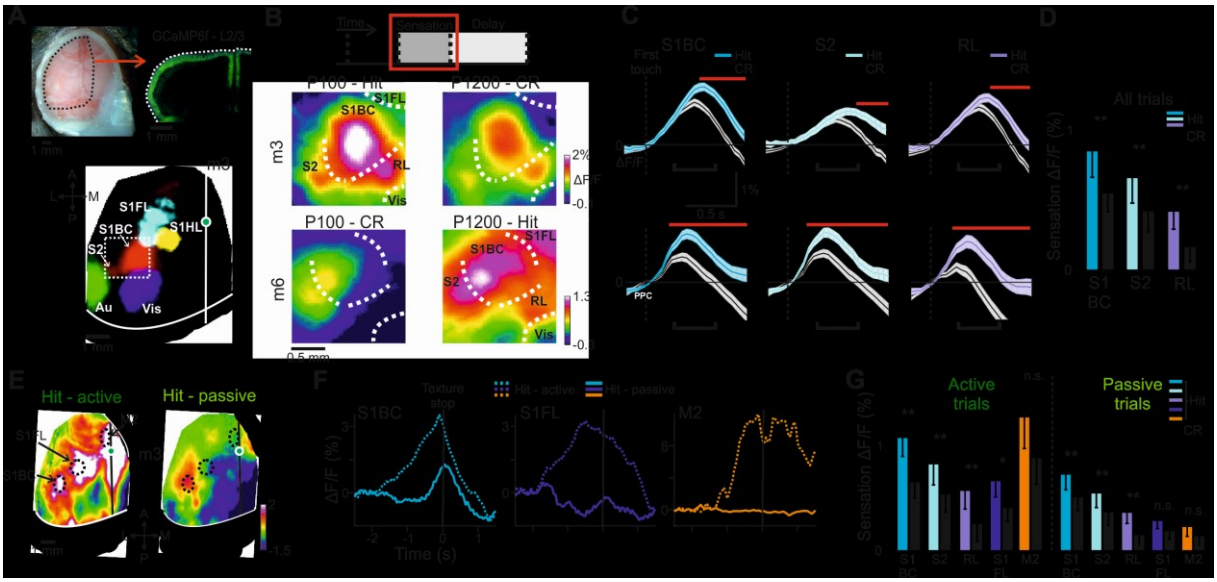

Figure 2. Posterior sensory areas encode choice early after touch independent of texture type and behavioral strategy.

(A) *Top left:* intact skull preparation. *Top right:* Confocal image of a coronal slice showing GCaMP6f (green) in L2/3 neurons. *Bottom:* Merged image of sensory-evoked activity maps indicating the different sensory areas. Colors indicate different sensory stimuli.

(B) Zoomed-in sensation maps for whisker-related posterior areas in hit and CR trials for two example mice, each trained on a different go texture (area corresponding to dashed white box in A; maps averaged from 0.3 to 0.7 s after first touch, gray bars in C). Color scale bar indicates min/max of percent ΔF/F.

(C) Mean ΔF/F traces of the examples in B in S1BC, S2 and RL. Error bars are s.e.m. across trials. Red lines indicate time frames with significant difference between hit and CR trials ($P < 0.05$; Mann-Whitney U-test). Black bars indicate time windows for calculation of sensation maps.

(D) Mean activation during sensation in S1BC, S2 and RL for hit versus CR trials averaged across all mice. Error bars are s.e.m. across mice (n = 8).

(E) Sensation maps for active (left) and passive (right) hit trials taken from the same imaging session in mouse #3. S1BC, S1FL, and M2 are outlined as dashed ovals.

(F) ΔF/F traces in S1BC, S1FL and M2 for the examples in E.

(G) Same as in D, but separated into active or passive trials and with the addition of S1FL and M2 areas. Error bars as in D. See also Figure S5A for a presentation of all areas.

$*P < 0.05$. $**P < 0.01$. $***P < 0.001$. n.s. not significant. Wilcoxon signed-rank test.

See also Figures S2-S5

We next asked if sensation maps depend on behavioral strategy by separating active and passive trials. For the same choice, e.g., in hit trials, this comparison revealed large differences. Sensation maps for active hit trials showed high activity in many areas—including whisker-related areas but also S1 forelimb area (S1FL) and secondary motor cortex M2—whereas activity in passive hit trials on the contrary was confined to S1BC, S2 and RL (Figure 2E, F). Pooled across all mice, activity in both active and passive trials was

significantly higher in hit versus CR trials in S1BC, S2, and RL (Figure 2G; $P < 0.05$; Wilcoxon signed-rank test; Figure S2D). In passive trials only, activities in S1FL and M2 (as well as whisking behavior) were low and not significantly different in hit versus CR trials (Figure 2G; $P > 0.05$; Wilcoxon signed-rank test). For active trials, S1FL activation (along with activation of other areas and whisking behavior) did show apparent differences, which we attribute to the different body movements observed in hit versus CR trials during sensation (see Figure S5A for a full description of activation levels during sensation in active versus passive trials for all areas examined in this study). Thus, consistent with previous reports (Chen et al., 2016; Yang et al., 2015), sensory-related posterior areas S1BC, S2 and RL encode choice shortly after touch for both behavioral strategies. In contrast, activity in the surrounding cortical areas exhibits large differences depending on behavioral strategy which may influence activation patterns during the delay period.

Distinct cortical areas hold information during the delay

We next analyzed which cortical areas are involved in short-term memory once the texture has been withdrawn, i.e., during the delay period (Figure 3). Since body movements evoke widespread activity we restricted this analysis to trials, in which the mouse was quiet for at least the first second during the delay. For the remaining delay period we excluded time periods when the mouse began to move because otherwise movement-related activity was evoked in many areas (Figure S6; STAR Methods). These criteria ensured that for both active and passive trials the analysis was not directly affected by movements because only time periods during the delay were considered when the mouse was sitting quietly and waiting for the response cue. From these quiet periods during the delay we created activity maps (‘delay maps’) with trials separated according to behavioral strategy, i.e., depending on whether the mouse had been active or passive earlier during sensation. As an example, mouse #6 typically alternated between strategies during imaging sessions. Surprisingly, delay maps were very

different for the two behavioral strategies, for individual hit trials as well as for whole-session averages (Figure 3A, B). In active trials, the delay map showed frontal activation (particularly in M2) whereas for passive trials the map displayed posterior activation, which was especially strong in a region just posterior and lateral to the visual cortex (Figure 3B; Figure S7; Videos S1-4). Based on anatomical maps of neocortex (Franklin and Paxinos; Wang et al., 2012) we refer to this region as 'posterior area P' (or brief 'P'; see Discussion; see also additional retinotopic alignment in Figure S7B). We emphasize that both active and passive trials used for generation of these delay maps were correct hit trials, so that stimulus identity, licking action and reward consumption were similar. For CR trials, the distinct patterns in active and passive delay maps were still discernible, albeit with much weaker contrast. In control experiments, we verified that these activity patterns were not confounded by hemodynamic signals, especially for the near-midline M2 area, which is close to the superior sagittal sinus (Figures S3 and S8).

We further analyzed how L2/3 calcium signals in S1BC, M2, and P differed between passive and active trials (Figure 3C). In active trials, due to body movements, ΔF/F traces were high prior and during the sensation period in all areas. Subsequently, M2 maintained high activity during the delay in hit but not in CR trials whereas other areas displayed a decrease below baseline. The latter observation suggests that posterior areas may be inhibited when information is maintained in M2 (Allen et al., 2017). In passive trials, the ΔF/F trace in M2 remained at baseline during the delay period whereas area P displayed enhanced activity, especially in hit trials.

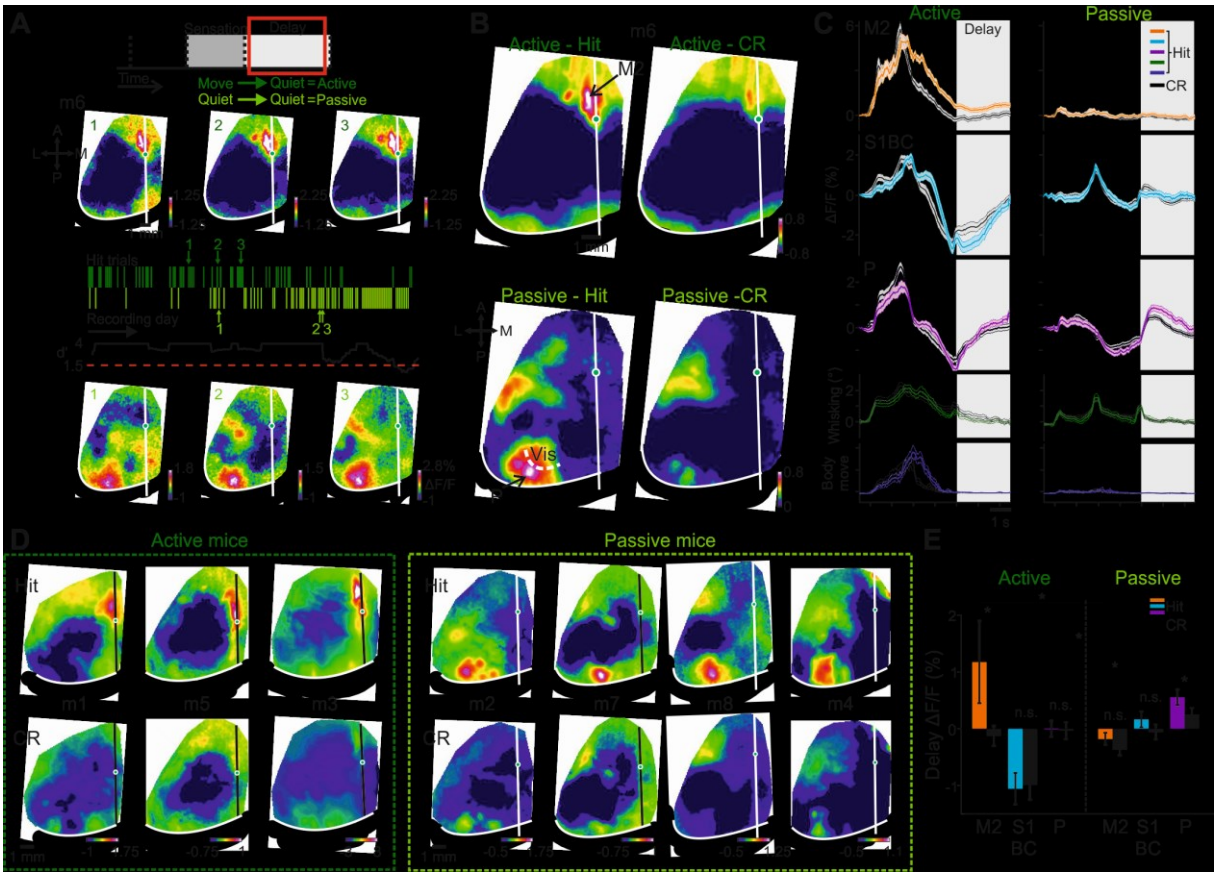

Figure 3. Diverging cortical activity during the delay depends on behavioral strategy.
(A) Example of one imaging day from mouse #6. Throughout the day the mouse displayed either an active (dark green) or passive (light green) strategy in hit trials while maintaining high performance (d' in black trace). Above and below are three examples of single-trial delay maps for active and passive strategies, respectively. Color scale bar indicates min/max of percent ΔF/F.
(B) Delay maps for the example day in A, averaged across the four trial types.
(C) Time courses of ΔF/F in M2, S1BC and P for the different trial types in B, along with body movement and whisker envelope. Error bars are s.e.m. across trials.
(D) Example session-average delay maps for the other mice in hit (top) and CR (bottom) trials sorted according to their activeness as shown in Figure 1F.
(E) Mean ΔF/F values during the delay period for hit and CR trials in M2, S1BC and P averaged across mice for active and passive trials. Error bars are s.e.m. across mice. See also Figure S5B for a presentation of all areas.
*$P < 0.05$. n.s. not significant. Wilcoxon signed-rank test.
See also Figures S3-S8

The distinct delay maps in active and passive trials—with patches of sustained activity in M2 and P, respectively—were consistent for all mice (Figure 3D). Also consistently, active mice showed P activation in their minority of passive trials and, vice versa, passive mice showed M2 activation in their few active trials (Figure S7D; $P < 0.05$; Wilcoxon signed-rank test). Other cortical areas did not show much difference between hit and CR trials (Figure

S5B). A quantitative comparison of hit versus CR trials pooled across mice revealed a significantly higher activation of M2 in active hit trials and of P in passive hit trials (Figure 3E; $P < 0.05$; Wilcoxon signed-rank test; n = 8 mice; Bonferroni corrected). For the less-preferred trial type (passive for M2 and active for P) the mean delay activity in these areas was low, although it sometimes showed remaining modulations that could still indicate some involvement (see example in Figure 3C). Delay activities in M2, S1BC, and P were also significantly different between active and passive hit trials (Figure 3E; $P < 0.05$; Wilcoxon signed-rank test; n = 8 mice; Bonferroni corrected). We like to remind again that during the delay time periods used for analysis mice were sitting quietly and waiting for the response cue. For both active and passive trials body movements remained below our movement threshold during these periods, with low accompanying whisking activity and no significant difference between hit and CR trials ($P > 0.05$; signed rank test for each mouse separately). In conclusion, we have discovered a divergence of neocortical dynamics that is contingent on behavioral strategy and leads to the activation of completely different areas during the delay period when information has to be maintained in short-term memory.

If distinct cortical areas hold relevant information for the future action, their activity should be discriminative for hit versus CR trials. To analyze the discrimination power during the delay, we trained a support vector machine (SVM) to classify between hit and CR trials based on all pixels in the imaging area (STAR Methods). SVM training was done for each imaging day and separately for active and passive trials (n = 4 and 5 mice, respectively). To exemplify this analysis we applied the SVM classifier only to two pixels during the delay period, one in M2 and the other in P. From the results, it is evident that for active trials the M2 pixel is most informative (i.e., is assigned a high weight), whereas for passive trials the P pixel is most informative (Figure 4A). When we performed SVM classification using all pixels in the imaging area (i.e. on the entire delay maps; 80% training; 20% testing; 20 cross-

validations), accuracy ranged from 60-88% in all mice for active and passive trials (Figure 4B).

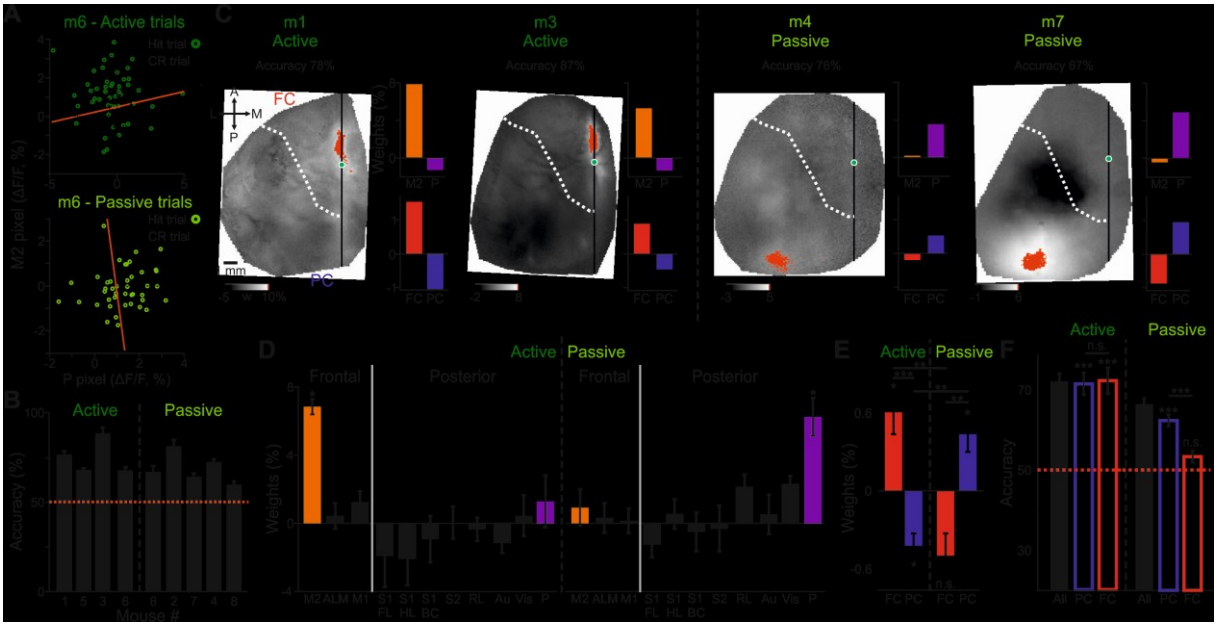

Figure 4. Location of hit vs. CR discrimination power in the delay period for passive or active strategies.
(A) An example showing responses (hit vs. CR trials) during the delay period in an M2 and a P pixel for active (top) and passive (bottom) trials. Red line indicates the linear separation between hit and CR trials derived from an SVM. In this example the M2 pixel can better classify in the active strategy whereas the P pixel can better classify in the passive strategy.
(B) SVM accuracy in classifying hit and CR single trial delay maps, shown for each mouse in active or passive strategy. Error bars are s.e.m. across imaging days.
(C) Four example weight maps in gray scale (two active and two passive). Top 1% weights are highlighted in red. Dashed white line indicates border between frontal and posterior cortex. Bar plots to the right show mean weights in the M2 and P areas (orange and purple, respectively) and the frontal and posterior cortex (red and blue, respectively; FC and PC).
(D) Weights in different areas for active and passive strategies pooled across mice. Error bars are s.e.m. across mice (n = 4 and 5 mice for active and passive strategies respectively).
(E) Same as d but for all pixels in the frontal or posterior cortex.
(F) SVM accuracies for active (left) and passive (right) strategy when using either all pixels (black), pixels only in the posterior cortex (blue) or pixels only in the frontal cortex (red). Error bars are s.e.m over imaging days (n = 31 from 4 mice for active strategy; n = 39 from 5 mice for passive strategy).
* $P < 0.05$. ** $P < 0.01$. *** $P < 0.001$. n.s. not significant. ANOVA and post-hoc analysis.
See also Figure S5C

We obtained 'weight maps' by assigning to each pixel its corresponding weight from the classifier. The best weights (top 1% highest absolute value) mapped to M2 or P for active and passive strategies, respectively (Figure 5C). Pooled across all mice, weights were significantly positive in M2 for active trials and in P for passive trials (Figure 4D; one-way

ANOVA; for active strategy $P < 0.001$; $F_{10,33} = 5.17$, 95% confidence interval (CI) [0.04 0.095] for M2; for passive strategy $P < 0.01$; $F_{10,44} = 2.86$, 95% CI [0.03 0.075] for P; n = 4 and 5 mice for active and passive strategies, respectively). Other areas displayed weights that did not significantly differ from zero (Figure 4D; $P > 0.05$ post-hoc). In addition, we analyzed the hit versus CR discrimination power for each area separately and obtained similar results (Figure S5C; STAR Methods). Dividing the cortical surface in frontal and posterior parts confirmed different fronto-posterior interactions based on behavioral strategy: In active trials frontal cortex was assigned significantly positive weight, whereas posterior cortex was assigned significantly negative weight (Figure 4E; one-way ANOVA; $P < 0.001$; $F_{3,14} = 13.8$; 95% CI $[3.6\ 10.2]\cdot10^{-3}$ for frontal cortex, 95% CI $[-8.1\ -1.5]\cdot10^{-3}$ for posterior cortex). In passive trials, weight distribution was the opposite (95% CI $[-5.7\ 0.13]\cdot10^{-3}$ for frontal cortex, 95% CI $[2.0\ 7.9]\cdot10^{-3}$ for posterior cortex). Interestingly, for passive trials, SVM accuracy was at chance level when we applied the SVM only to pixels in the frontal cortex (Figure 4F; $P > 0.05$; signed-rank test compared to 50%; Bonferroni corrected; n = 39 imaging sessions from 5 passive mice). Significant accuracy was maintained when using only pixels in the posterior cortex ($P < 0.001$; signed-rank test compared to 50%; Bonferroni corrected). For active trials, in contrast, accuracy remained high when using either frontal or posterior pixels only (Figure 4F; $P < 0.001$; signed-rank test compared to 50%; Bonferroni corrected; n = 31 imaging sessions from 4 active mice). This finding is explained by the relatively wide-spread decrease in activity seen in posterior cortex during hit trials. These results indicate that at least in some cases (e.g., during a passive strategy) short-term memory is not maintained in frontal cortex.

Cellular-resolution imaging substantiates strategy-dependent M2 and P activation

To corroborate the wide-field population signal we additionally used two-photon imaging to resolve single-cell activity while mice performed the task. Guided by the wide-field maps we targeted regions of interest that displayed high activation (Figure 5A). Specifically, we implanted 5 of the 8 mice with a glass window above either posterior areas (S1BC, S2, RL and P; mice #5 and 8) or frontal areas (M2; mice #3, 4 and 6). Both types of windows included at least one active and one passive mouse. Consistent with the wide-field data in Figure 2, L2/3 neurons in S1BC, S2 and RL displayed significantly higher activity in hit versus CR trials during the sensation period (Figure 5B, C; $P < 0.05$ signed rank test). During the delay period, M2 displayed a significantly higher fraction of responsive L2/3 neurons and larger average responses in hit trials for active but not passive mice (Figure 5D-F; $P < 0.05$; signed rank test). In contrast, P displayed significantly more responsive L2/3 neurons and larger responses in hit trials for passive but not active mice (Figure 5G-I; $P < 0.05$; signed rank test).

In addition, we analyzed the discrimination power between hit and CR for individual L2/3 neurons. We found that M2 neurons were more discriminative in active compared to passive trials, whereas P neurons were more discriminative in passive trials (Figure S5D). Moreover, M2 contained a higher fraction of significantly discriminating cells in active trials whereas in area P more discriminative cells were present in passive trials (Figure S5E). A vast majority of discriminative cells preferred the hit condition. These analyses confirm the results from our population-level analyses based on wide-field imaging data and additionally indicate that M2 and P display relatively homogeneous dynamics within the neuronal populations during the delay period.

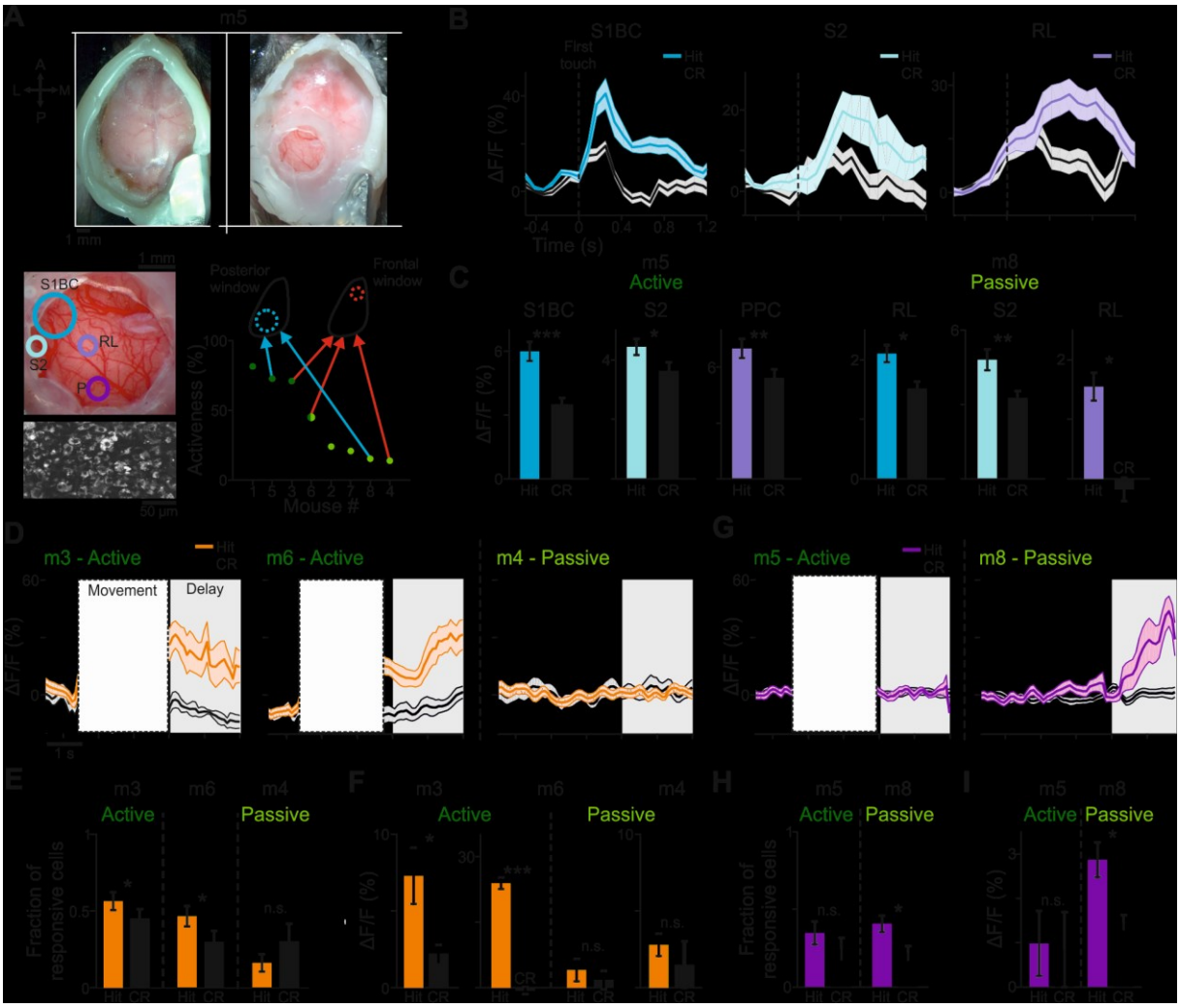

Figure 5. Single-cell two-photon imaging confirms wide-field calcium imaging results.
(A) *Top images:* wide-field preparation of mouse #5 with (right) and without (left; both images are aligned) a posterior cranial window for targeting single cells in the same mice used for wide-field imaging. *Bottom left:* Enlargement of the cranial window with four ROIs outlined. Below is an example two-photon field of view from S1BC. *Bottom right:* two mice (#5, 8) were implanted with a posterior window (S1BC, S2, RL and P areas) and three mice were implanted with an anterior window over M2 (#3, 4, 6).
(B) Example cells during the sensation period from S1BC, S2 and RL for hit and CR trials (mouse #5). Error bars s.e.m. over trials.
(C) Activation during the sensation period in the three areas shown for each mouse separately. Error bars s.e.m. over cells.
(D) Three example M2 cells from two active mice (#3, 6) and one passive mouse (#4) with a frontal window. Movement periods in active mice during sensation are omitted due to movement artifacts. Error bars s.e.m. over trials.
(E) Fraction of responsive M2 cells for hit or CR conditions during the delay for the three mice. Error bars are s.e.m. over cells.
(F) M2 activation during the delay for the three mice in active or passive trials. Error bars as in E.
(G-I), Same as D-F but for the P area in two mice (one active and one passive). $*P < 0.05$, $**P < 0.01$, $***P < 0.001$, n.s. not significant. Wilcoxon signed-rank test.
See also Figure S5D, E

Perturbing P or M2 impairs performance and can induce strategy switches

Next, we tested whether the activation patches observed in area P and M2 during the delay period are behaviorally relevant. We trained a new batch of L2/3-GCaMP6f mice (n = 6) that reached high performance with activeness ranging from 29-92% (Figure 6A). Body movements were monitored and analyzed as before. Delay maps from baseline imaging sessions again revealed sustained activation in M2 and P in active and passive mice, respectively (Figure 6B). Next, depending on the mouse's main strategy, we targeted either M2 or P for injection of AAV-CAG-ArchT-GFP to locally express Archaerhodopsin (ArchT), an optical neural silencer (Han et al., 2011; STAR Methods). After 4-5 weeks mice were re-trained and then performed the task while green light (561 nm) was delivered to the injected region during the delay period randomly in 50% of the trials ('perturbation sessions'; STAR Methods). After these sessions, mice continued in further wide-field imaging sessions without light delivery and for additional controls ('post sessions'; STAR Methods). The timeline of experiments thus covered 14-25 weeks per mouse (Figure 6C). Our working hypothesis was that ArchT activation during the delay period would either impair performance or induce a change in strategy or both. In addition, we expected M2 and P perturbations to be most effective during active and passive trials, respectively.

We first show examples of 3 mice, each exhibiting a different effect. In the first example, mouse #13 was perturbed in area P which resulted in a significant decrease in performance in the trials with light delivery ($P < 0.01$; signed-rank test), dropping to a performance level not significantly different from our expert threshold of d' = 1.5 (Figure 6D*i*: $P > 0.05$ d' compared with 1.5; signed-rank test). The mouse maintained its passive strategy when comparing baseline and perturbation sessions (Figure 6D*ii*; trials with and without light pooled together; $P > 0.05$; Wilcoxon rank test). Importantly, when separating trials into active and passive trials, the reduction in performance caused by ArchT activation only occurred in passive trials (Figure 6D*iii*; $P < 0.01$; signed-rank test).

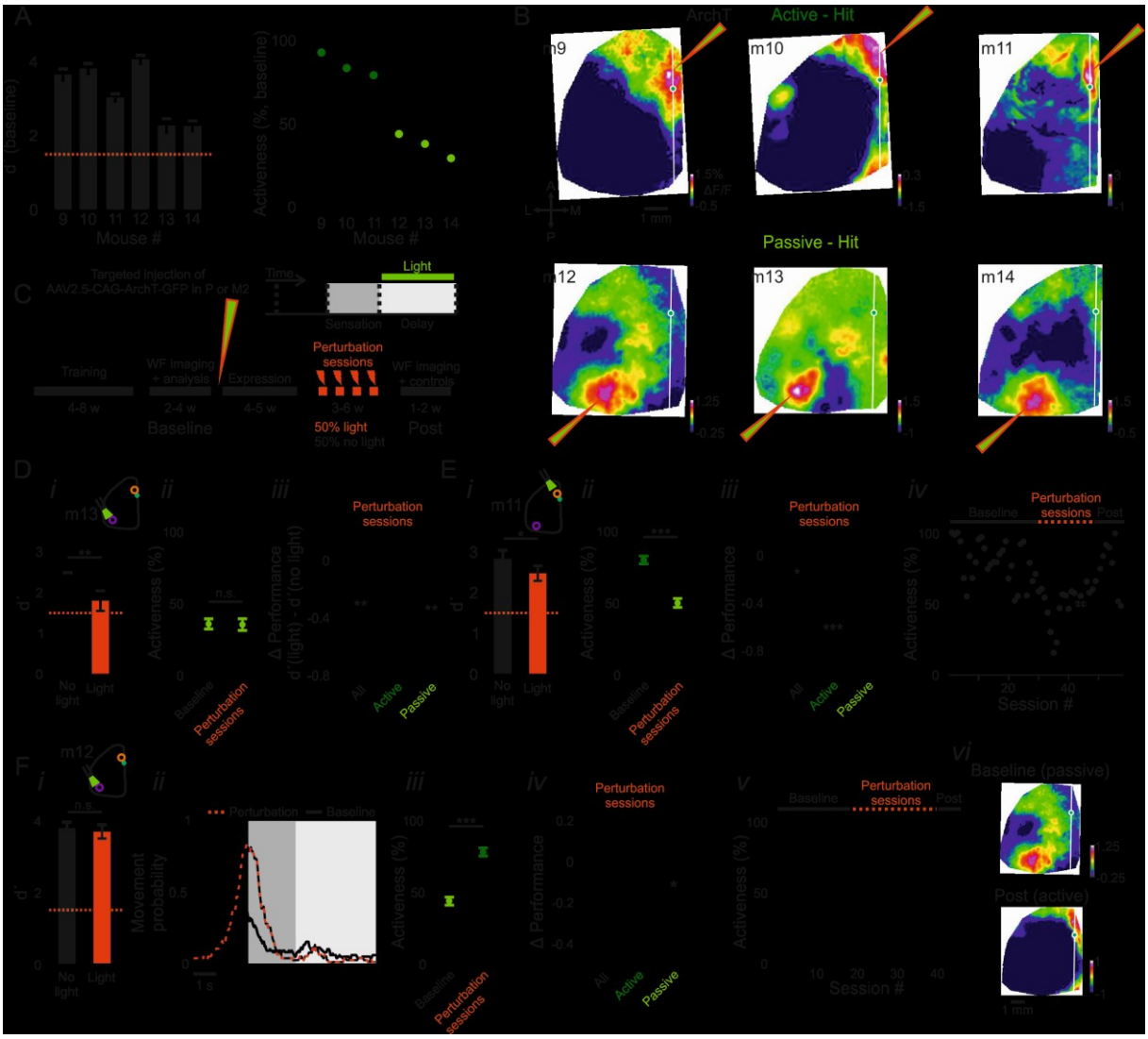

Figure 6. Perturbation of M2 or P causes drop in performance and/or change in strategy.

(A) Performance and activeness of additional mice used in optogenetic experiments. 3 mice were labelled as active and 3 as passive.

(B) Delay maps for the 6 mice showing activation patches in M2 or P depending on the mouse's main strategy. Pipettes indicate targeted injection sites for ArchT-expressing virus.

(C) Time line of experiment in weeks. *Top right:* timing of light delivery during the trial

(D) Example from mouse #13 (passive), perturbing area P. *i,* Performance during perturbation sessions with and without light. *i,*. Mean activeness during baseline and perturbation sessions. *ii,*. Difference in performance (ΔPerformance = d'(light) – d'(no-light)) for all trials and for active or passive trials separately.

(E) Example from mouse #11 (active), perturbing area M2. Panels *i-iii* as in d. *iv,* Activeness in each recording session throughout the experiment.

(F) Example from mouse #12 (passive), perturbing area P. Panels *i, iii, iv* and *v* as in E. *ii*, Probability of movement for an example baseline and perturbation session (trials with and without light pooled). *vi,* Example delay map taken during baseline (top; in passive trials) and during post sessions (bottom; in active trials). Error bars are s.e.m. across recording sessions. $*P < 0.05$, $**P < 0.01$, $***P < 0.001$, n.s. not significant. Wilcoxon signed-rank test or Mann-Whitney U-test.

See also Figure S9

In the second example, mouse #11 was perturbed in M2 and showed a small but significant decrease in performance due to light delivery (Figure 6E*i*: $P < 0.05$; signed-rank test), though still remaining above expert threshold ($P < 0.001$, signed-rank test). Interestingly, this mouse showed more passive behavior in perturbation sessions compared to baseline sessions (Figure 6E*ii*: $P < 0.05$; Mann-Whitney U-test). Different from mouse #13 and consistent with perturbation in M2, performance decreased significantly only in the perturbed active trials (Figure 6E*iii*: $P < 0.001$; signed-rank test). By switching its strategy to more passive behavior this mouse apparently partially compensated for the performance drop. Activeness stayed reduced during perturbation sessions but the mouse quickly shifted back to higher activeness in post-sessions (Figure 6E*iv*).

The third example mouse #12 was perturbed in area P but overall performance did not significantly decrease (Figure 6F*i*: $P > 0.05$; signed-rank test). Notably, however, this mouse very efficiently switched its strategy from passive to active in the perturbation sessions (Figure 6F*ii*, *iii*; $P < 0.001$; Mann-Whitney U-test). While perturbation of area P still reduced performance significantly in the passive trials, these were now less abundant compared to the unaffected active trials (Figure 6F*iv*; $P < 0.05$; signed-rank test). Following the perturbation sessions, this mouse maintained an active strategy in post-sessions (Figure 6F*v*). Correspondingly, the main delay map switched from P to M2 activation for baseline compared to post sessions (Figure 6F*vi*).

The other 3 mice followed one of the above scenarios (Figure S9). Taking all mice together, we found that mice that tended to maintain their strategy displayed the strongest reduction in performance upon ArchT activation (Figure 7A). Interestingly, we found a significantly positive correlation between the baseline performance of mice and their ability to switch strategies (Figure 7B), indicating that the best performing mice were also more flexible. Importantly, the 3 mice silenced in M2 showed a significant impairment in performance only in active trials whereas the 3 mice that were silenced in P showed a

significant impairment only in passive trials (Figure 7C). In summary, perturbation of one area (M2 or P) decreased performance exclusively when the mouse used the associated strategy (Figure 7D; $P < 0.05$; signed-rank test). Some mice flexibly overcame the perturbation by switching to an alternative strategy, shifting short-term memory location to the unperturbed area, whereas others did not make use of this option (see Discussion).

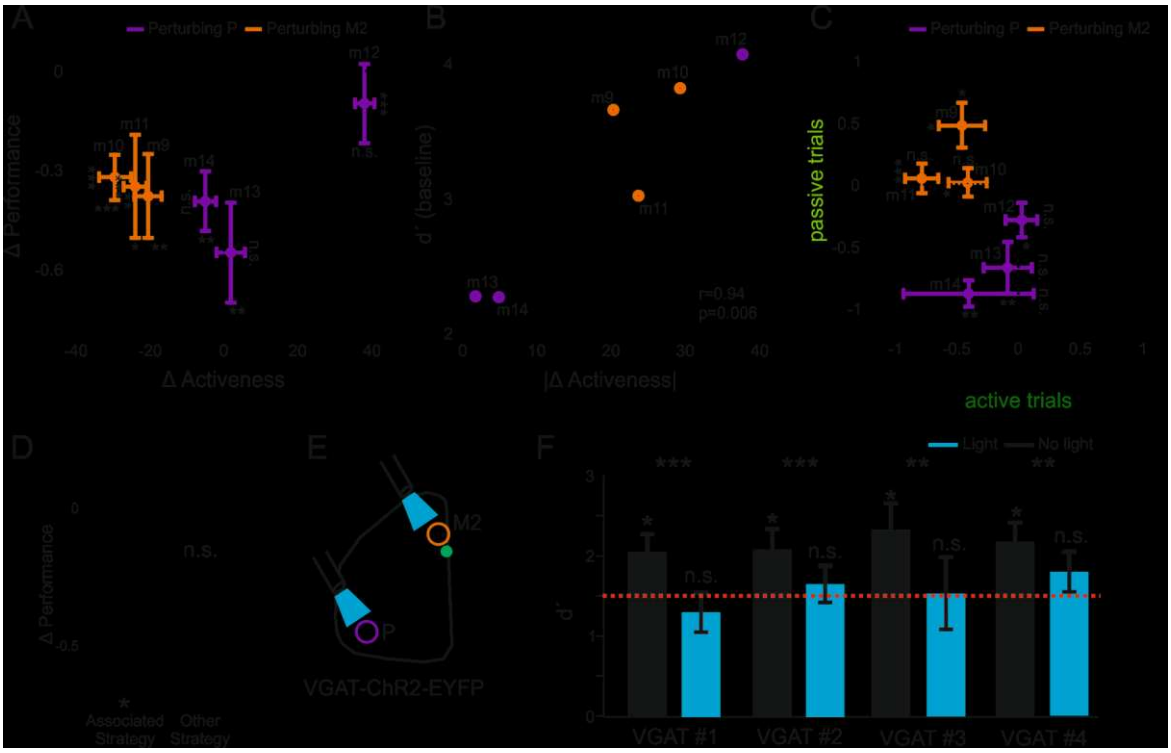

Figure 7. Perturbation of M2 and P areas impairs expert level performance.
(A) For each mouse, ΔPerformance (d'(light) – d'(no-light)) is plotted versus the change in activeness from baseline to perturbation sessions (ΔActiveness; activeness in perturbation sessions minus activeness in baseline sessions). Orange and purple indicate perturbation of M2 and P, respectively.
(B) Performance in baseline sessions as a function of absolute change in activeness for each mouse (|activeness in perturbation minus activeness in baseline sessions|).
(C) ΔPerformance in passive versus active trials for each mouse.
(D) ΔPerformance for the strategy associated with the perturbed area (i.e. active strategy for M2 and passive strategy for P) and during the other strategy.
(E) Simultaneous silencing of both M2 and P in mice expressing ChR2 in GABAergic neurons during the delay period.
(F) Performance (d') of 4 VGAT-ChR2 mice without (black) and with (blue) light to perturb both M2 and P. Dashed red line marks expert level threshold.
Error bars are s.e.m. across recording sessions except for panel D where error bars are s.e.m. across mice. *$P < 0.05$, **$P < 0.01$, ***$P < 0.001$, n.s. not significant. Wilcoxon signed-rank test or Mann-Whitney U-test.

If short-term memory requires activation of either P or M2, then silencing both areas should strongly impair performance. To test this idea, we trained 4 additional VGAT-ChR2-EYFP mice expressing channelrhodopsin-2 (ChR2) in GABAergic interneurons throughout the cortex (Zhao et al., 2011). Mice underwent the same training procedure. After reaching expert level both M2 and P areas were silenced simultaneously during the delay period (Figure 7E; STAR Methods). All four mice significantly reduced their performance upon ChR2 activation ($P < 0.001$; signed-rank test), down to levels not significantly different from the expert threshold (Figure 7F; $P > 0.05$; signed-rank test). In summary, our optogenetic perturbation experiments confirm the hypothesis that M2 and P are necessary for maintaining task-relevant information in short-term memory and that their essential role is bound to the respective active and passive strategy.

M2 and P maintain motor- and sensory-related information, respectively

Finally, we investigated what type of information is maintained in M2 and P during the delay period. Using a go/no-go task the information maintained during the delay can be related to either past stimulus identity or future motor action. To dissociate between these two possibilities, we analyzed the error trials, i.e. false alarm (FA) and Miss trials, and compared them to hit and CR trials. Similar to correct trials, error trials were separated into active and passive trials for each mouse. In general, activeness in both FA and Miss trials was similar to hit trials, with a tendency to reduced activeness, especially for Miss trials (Figure 8A; mean activeness across all mice: 42.8, 35.9 and 32.3% for hit, FA, and Miss trials). Next, we calculated the mean activity during the delay period in M2 and P for each error type in active and passive trials. Similar to hit trials (see Figure 3E) delay activity tended to display positive values in M2 during active trials and in P during passive trials for both FA and Miss trials (Figure 8B).

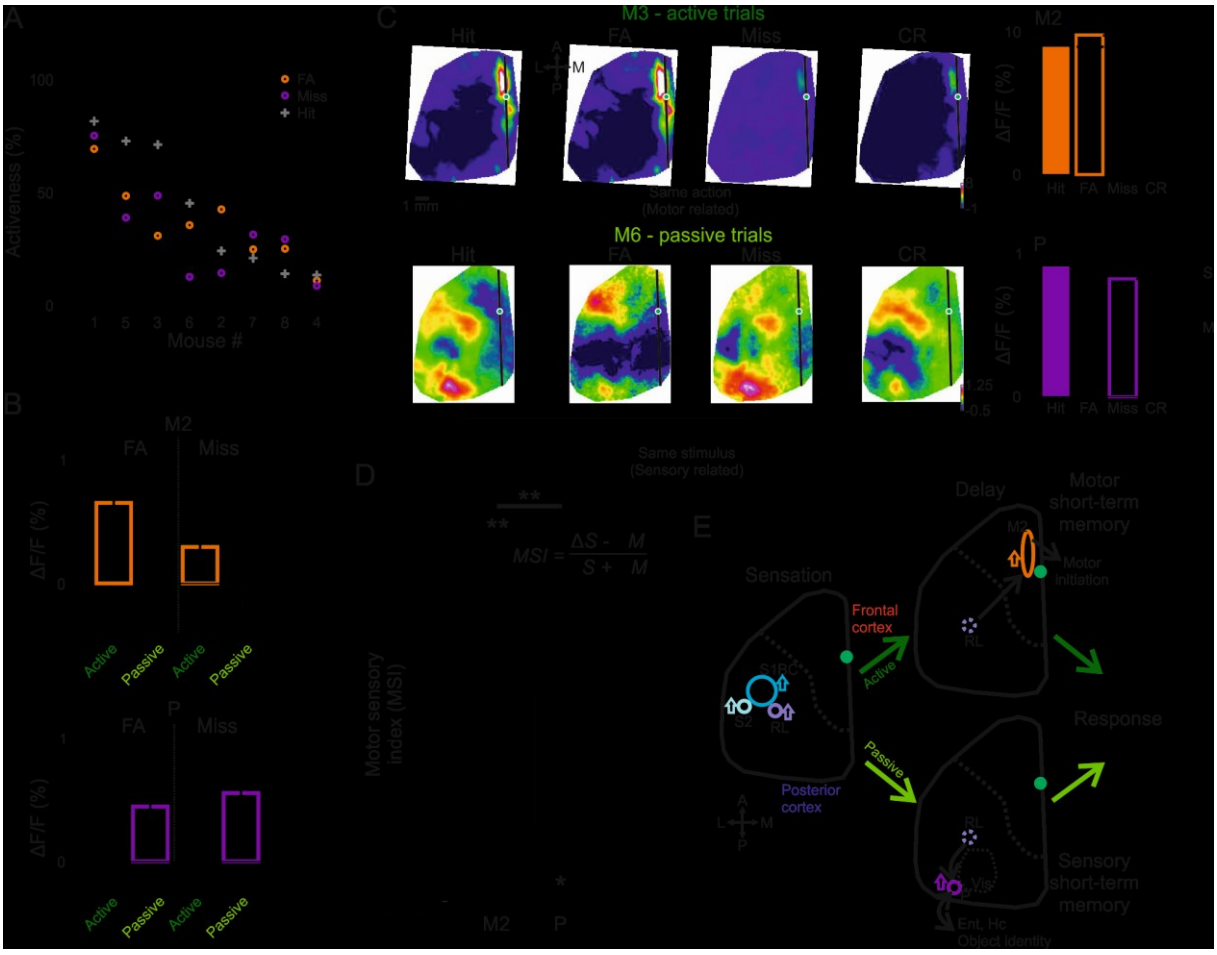

Figure 8 Short-term memory is motor-related in M2 and sensory-related in P

(A) Activeness for each mouse during FA (orange) and Miss (purple) trials. Gray crosses indicates the activeness for each mouse (calculated for hit trials; Similar to Figure 1F).

(B) Mean ΔF/F values during the delay period in M2 (top) and P (bottom) for FA and Miss during active and passive trials. Error bars are s.e.m across mice (n = 8).

(C) Top row: Example delay maps for Hit, FA, Miss and CR during active trials. On the right, mean ΔF/F values in M2 are shown for each trial type. In this example, trials with similar action display similar responses in M2. Bottom row: Same as the top row but for passive trials. Here, trials with similar stimulus display similar ΔF/F responses in P.

(D) Motor-sensory index (MSI) in M2 and P. Error bars are s.e.m across mice (n = 8). $*P < 0.05$, $**P < 0.01$, Wilcoxon signed-rank test.

(E) Hypothesized cortical dynamics during sensation and short-term memory. During the sensation period, a posterior network (S1BC, S2, and RL) displays enhanced activity enabling the discrimination between the two textures. At the beginning of the delay period, information presumably flows to either frontal or posterior areas for short-term maintenance depending on the mouse's strategy: from RL to M2 during an active strategy ('motor short-term memory') or from RL to P during a passive strategy ('sensory short-term memory'). Both cortical states eventually converge to trigger a similar behavioral response (licking the water spout). Ent – Entorhinal cortex. Hc – Hippocampus.

Next, we compared M2 delay activity for all choice types in active trials. In an example active session, the delay map for FA was similar to hits and the one for Misses was similar to CR, all showing M2 activation (Figure 8C; top). Thus, maps for active trials with

similar future action (lick or no-lick) displayed similar activation in M2. For passive trials, in contrast, delay maps and the corresponding activation of P were similar for trial types with the same past sensory stimulus, with hits resembling Misses and FA resembling CR (Figure 8C; bottom). To quantify this difference we defined a motor-sensory index (MSI) taking into account for each error type whether its delay map was more similar to the correct-trial map with same past stimulus identity or the one with same future motor action (STAR Methods). MSI ranges from -1 to 1 where positive values indicate motor-related information content whereas negative values indicate maintenance of sensory-related information. MSI was calculated for each mouse separately in M2 for active trials and in P for passive trials. MSI was significantly positive in M2 and significantly negative in P (Figure 8D; $P < 0.05$; Wilcoxon signed-rank test), implying that each area encodes a different type of short-term memory (see Discussion). In summary, M2 activity holds information related to the future action, whereas P activity holds information related to the past sensory stimulus.

DISCUSSION

We have shown that mice can deploy either an active or passive strategy to solve a texture discrimination task. Upon texture touch, whisker-related areas in posterior cortex (S1BC, S2, and RL) encode the choice of the mouse independent of strategy. During the delay period we find a clear divergence of activity patterns to either M2 or P depending on behavioral strategy. In addition, M2 is more related to the future motor action whereas P is more related to the past stimulus identity. We propose that short-term memory is present in two different forms: motor-related memory in M2 or sensory-related memory in P (Figure 8E). Furthermore, holding information about texture identity in P may be part of the “what” pathway whereas actively approaching the object with whisking and body movement may be related to engaging the “where” pathway (Diamond et al., 2008; Van Essen and Gallant, 1994; Goodale and Milner, 2003), as also suggested by a previous anatomical study in mice (Wang et al.,

2012). Nevertheless, additional experiments directly testing each pathway will be needed to substantiate these ideas.

M2 is presumed to play a role in sensory integration via top-down influences (Manita et al., 2015; Schneider et al., 2014; Zhang et al., 2014) as well as in action planning (Erlich et al., 2011; Murakami et al., 2016; Siniscalchi et al., 2016). We find that M2 also encodes short-term memory, but only for the active strategy. In passive trials, M2 as well as other frontal areas (including ALM; Guo et al., 2014; Li et al., 2015) were not activated and could not discriminate trial types (Figure 4), suggesting that they are less important for maintaining information for this type of behavior, at least before any preparatory movements. We emphasize that in our analysis we excluded preparatory stereotypic movements initiated before the licking response (Otchy et al., 2015) as these movements typically activate many frontal areas, including M2 and ALM (Figure 2E; Figure S5). Future studies of frontal cortical dynamics thus should carefully take into account behavioral parameters that may indirectly affect the results. It will be interesting to investigate in detail how cortical activity may shift from posterior to frontal areas during the transition phase at the start of preparatory movements.

In passive trials we discovered that a less studied lateral posterior area maintains hit/CR information during short-term memory. The center location of this area best matches to area P (Wang et al., 2012), also referred to as posterolateral area (Lein et al., 2007) or lateral secondary visual cortex (Franklin and Paxinos). Given the variability among animals, however, the observed activation spot may also encompass adjacent posterior areas such as lateromedial visual cortex or postrhinal cortices. Area P so far has been mainly implied in visual processing (Wang and Burkhalter, 2007; Zhuang et al., 2017). It is reciprocally connected to parahippocampal, temporal and parietal cortices (Oh et al., 2014; Wang et al., 2012). We suggest that P processes information about object identity, receiving tactile

information presumably via RL and encoding relevant features as part of the "what" pathway (Figure 8E). It also could be involved in a comparison with internal long-term memory retrieved by hippocampus (Felleman and Van Essen, 1991). Area P may be a homologue to primate lateral occipito-temporal complex (LOC), which is thought to process hapto-visual information (Amedi et al., 2002). In active trials, this pathway may be less engaged since information is rapidly shifted to motor-related areas. In area P we find similarly high activity during the delay in passive Miss and hit trials, indicating that P holds sensory-related information. This was also true at the end of an imaging day when some mice appeared less motivated, implying that sensory information was stored in P despite the mouse not licking for reward. In this context, we find that active mice initiate preparatory movements earlier than passive mice, consistent with the idea that short-term memory in frontal areas is more motor-related and that movements may help to transform cortical activity for action preparation (data not shown).

We defined behavioral strategies based on obvious body movement during sensation but differences between active and passive mice could also reflect attentional, arousal, or motivational state. To dissociate between these states and behavioral strategy we emphasize several points. First, even though activeness fluctuated most mice generally maintained similar activeness levels across days and weeks, consistent with the notion that mice adopt a particular strategy, i.e., plan their action to maximize reward and/or minimize energy consumption. Second, when perturbing only one area (M2 or P) some mice adopted an alternative strategy (while maintaining high performance), changing their activeness also in trials where no light was delivered. Third, despite a correlation between performance level and activeness passive mice still performed at high levels in both strategies (Figure 1F). Fourth, in some cases active and passive hit trials were intermingled within a session (e.g., Figure 3A), again implying that the general attentional state and motivation of the animal were similar. Fifth, in many cases activeness did not change across the imaging day (Figure

S1F). Thus, attentional, arousal, or motivational states are less likely to be exclusively related to the observed cortical activity patterns. Another concern may be that the go/no-go task design is biased to the go-condition in terms of reward consumption, motor plan and preparation, making it difficult to relate the observed cortical delay maps to short-term memory. We emphasize, however, that our major finding is a prominent difference between delay maps for two types of hit trials (active vs. passive). In both types of hit trials the mouse is sitting quietly and waiting for the response cue after the texture has been retracted. In addition, texture identity, licking action, and reward consumption are similar in all hit trials. Future studies could aim to further reveal how internal parameters (e.g. motivation, arousal, and energy constraints) as well as external parameters (e.g. stimulus type or location in space) may shape different behavioral strategies. Specifically, a delayed match-to-sample task where the decision is contingent on the comparison of two temporally spaced stimuli (recently also established in rodents; Fassihi et al., 2014, 2017; Liu et al., 2014) can better dissociate between maintenance of sensory information in working memory from processes involved in decision making and motor planning. It remains to be seen how our results will compare to patterns of persistent activity observed during the delay period in such a task.

Are the distinct activation patches in M2 and P causally linked to the mouse's ability to perform the task? Often causality is tested by demonstrating a reduction in task performance upon silencing of individual or several cortical areas (Allen et al., 2017; Goard et al., 2016; Guo et al., 2014; Kamigaki and Dan, 2017; Licata et al., 2017). Here, we find that some mice manage to maintain relatively high performance despite perturbation of one area (M2 or P) whereas other mice show significantly reduced performance. The former mice apparently flexibly switch to the alternative unperturbed strategy whereas the latter mice maintain their strategy. Strategy switches were consistent across days, present also in trials without perturbation and were clearly reflected in corresponding switches between M2- and P-dominated delay maps. Importantly, all mice showed impaired performance only during the

strategy associated with the perturbed area and not during the alternative strategy, demonstrating a strategy-specific effect. In conclusion, some mice (likely the best performing) are able to overcome strategy-specific perturbation by re-routing information via other cortical pathways and thus optimizing their reward. This option is not available when perturbing both M2 and P, in which mice reduced performance to non-expert level, implying that both areas together are necessary for maintaining short-term memory.

What mechanisms could underlie differential routing of cortical activity? In mice, posterior parietal cortex—including RL, which we studied here, as well as more medial areas such as anterior area A and anteromedial area AM (Wang et al., 2012; Zhuang et al., 2017)—plays a pivotal role in sensory integration for different sensory modalities (Goard et al., 2016; Harvey et al., 2012; Jeong et al., 2017; Marcos and Harvey, 2016; Raposo et al., 2014). Whether these areas maintain information during a delay is less clear, as this has been implicated in some (Harvey et al., 2012) but not in other studies (Erlich et al., 2015; Goard et al., 2016; Guo et al., 2014). Neuronal populations in RL project both to frontal M2 and to posterior areas including area P (Oh et al., 2014; Wang et al., 2012; http://connectivity.brain-map.org/). Therefore, they could route information to either frontal or posterior cortices depending on the mouse's state. The divergence of RL projections fits well with our finding that short-term memory is maintained in distinct cortical patterns based on behavioral strategies. We therefore hypothesize that RL could act as a key routing area (Figure 8E).

In this study, we used mainly wide-field imaging to reveal areas of interest that are involved in cortical processing. The advantage of this method is the simultaneous and unbiased sampling of large parts of the cortex, which enables identification of areas that did not gain previous attention (e.g. area P). The disadvantage of the method is that the wide-field fluorescence signals represent bulk signals, summed over neuronal populations (as well as potentially confounded by non-neuronal fluorescence changes, which needs to be controlled for). We therefore cannot exclude the possibility that we have missed intermingled sub-

populations of neurons that carry task-relevant information but are averaged out in the population signal. In addition, this study focused on layer 2/3 neurons, whereas other layers may contribute differently to task-related processes (Chandrasekaran et al., 2017; van Kerkoerle et al., 2014; Li et al., 2015). In summary, our results highlight the importance of taking into account global behavioral parameters and accounting for the individuality of subjects when studying cortical dynamics. Maintenance of information in short-term memory is not necessarily tied to one cortical area but is flexibly localized according to behavioral strategy (Leavitt et al., 2017). This flexibility reflects that the same behavioral outcome can be achieved in different ways.

ACKNOWLEDGMENTS

We thank Rodrigo C. Lentini, Balazs Laurenczy, Jonathan Schaffner, Sreedevi Madhusudhanan, Christopher Lewis, Stewart Berry, Pia Sipilä and Dayra A. Lorenzo for help with data analysis; Lazar Shumanovski for help with histology; Ladan Egolf for managing transgenic mouse lines; and David Margolis, Christian Ruff, Jerry L. Chen, and Inbal Ayzenshtat for comments on the manuscript. This work was supported by grants from the Swiss National Science Foundation (31003A-149858; F.H.), the European Research Council (ERC Advanced Grant BRAINCOMPATH, project 670757; F.H.), the Edmond and Lily Safra Center for Brain Sciences (ELSC) postdoctoral fellowship (A.G.), an EMBO long-term postdoctoral fellowship (ALTF_1077-2014; A.G.) and a Marie-Curie Individual Fellowship (659719-AG-GF; A.G.).

AUTHOR CONTRIBUTIONS

A.G. and F.H. designed the experiments, A.G., Y.G. and D.G. conducted the experiments, A.G., Y.G. and F.H. analyzed the data, A.G. and F.H. wrote the paper.

DECLARATION OF INTERESTS

The authors declare no competing interests.

REFERENCES

Allen, W.E., Kauvar, I. V., Chen, M.Z., Richman, E.B., Yang, S.J., Chan, K., Gradinaru, V., Deverman, B.E., Luo, L., and Deisseroth, K. (2017). Global Representations of Goal-Directed Behavior in Distinct Cell Types of Mouse Neocortex. Neuron *94*, 891–907.e6.

Amedi, A., Jacobson, G., Hendler, T., Malach, R., and Zohary, E. (2002). Convergence of Visual and Tactile Shape Processing in the Human Lateral Occipital Complex. 1202–1212.

Chandrasekaran, C., Peixoto, D., Newsome, W.T., and Shenoy, K. V. (2017). Laminar differences in decision-related neural activity in dorsal premotor cortex. Nat. Commun. *8*.

Chen, J.L., Carta, S., Soldado-Magraner, J., Schneider, B.L., and Helmchen, F. (2013). Behaviour-dependent recruitment of long-range projection neurons in somatosensory cortex. Nature *499*, 336–340.

Chen, J.L., Voigt, F.F., Javadzadeh, M., Krueppel, R., and Helmchen, F. (2016). Long-range population dynamics of anatomically defined neocortical networks. Elife *5*, 1–26.

Chen, T.-W., Li, N., Daie, K., and Svoboda, K. (2017). A Map of Anticipatory Activity in Mouse Motor Cortex. Neuron *94*, 866–879.e4.

Churchland, M.M., Cunningham, J.P., Kaufman, M.T., Foster, J.D., Nuyujukian, P., Ryu, S.I., and Shenoy, K. V (2012). Neural population dynamics during reaching. Nature *487*, 51–56.

Diamond, M.E., von Heimendahl, M., Knutsen, P.M., Kleinfeld, D., and Ahissar, E. (2008). "Where" and "what" in the whisker sensorimotor system. Nat. Rev. Neurosci. *9*, 601–612.

Erlich, J.C., Bialek, M., and Brody, C.D. (2011). A cortical substrate for memory-guided orienting in the rat. Neuron *72*, 330–343.

Erlich, J.C., Brunton, B.W., Duan, C.A., Hanks, T.D., and Brody, C.D. (2015). Distinct

effects of prefrontal and parietal cortex inactivations on an accumulation of evidence task in the rat. Elife *4*, 1–28.

Van Essen, D.C., and Gallant, J.L. (1994). Neural mechanism of form and motion processing in the primate visual system. Neuron *13*, 1–10.

Fassihi, A., Akrami, A., Esmaeili, V., and Diamond, M.E. (2014). Tactile perception and working memory in rats and humans. Proc. Natl. Acad. Sci. U. S. A. *111*, 2331–2336.

Fassihi, A., Akrami, A., Pulecchi, F., Schönfelder, V., and Diamond, M.E. (2017). Transformation of Perception from Sensory to Motor Cortex. Curr. Biol. *27*, 1585–1596.e6.

Felleman, D.J., and Van Essen, D.C. (1991). Distributed hierarchical processing in the primate cerebral cortex. Cereb. Cortex *1*, 1–47.

Ferezou, I., Haiss, F., Gentet, L.J., Aronoff, R., Weber, B., and Petersen, C.C.H. (2007). Article Spatiotemporal Dynamics of Cortical Sensorimotor Integration in Behaving Mice. 907–923.

Franklin, K.B.J., and Paxinos, G. Paxinos and Franklin's The mouse brain in stereotaxic coordinates.

Garner, A.R., Rowland, D.C., Hwang, S.Y., Baumgaertel, K., Roth, B.L., Kentros, C., and Mayford, M. (2012). Generation of a Synthetic Memory Trace. Science (80-.). *335*, 1513–1516.

Gilad, A., Meirovithz, E., and Slovin, H. (2013). Population Responses to Contour Integration: Early Encoding of Discrete Elements and Late Perceptual Grouping. Neuron *78*, 389–402.

Goard, M.J., Pho, G.N., Woodson, J., and Sur, M. (2016). Distinct roles of visual, parietal,

and frontal motor cortices in memory-guided sensorimotor decisions. Elife *5*, 1–30.

Goodale, M.A., and Milner, A.D. (2003). 1 2 Separate Visual Pathways for Perception and Action. Essent. Sources Sci. Study Conscious. 175.

Gossen, M., and Bujard, H. (1992). Tight control of gene expression in mammalian cells by tetracycline-responsive promoters. Proc. Natl. Acad. Sci. U. S. A. *89*, 5547–5551.

Guo, Z. V, Li, N., Huber, D., Ophir, E., Gutnisky, D., Ting, J.T., Feng, G., and Svoboda, K. (2014). Flow of cortical activity underlying a tactile decision in mice. Neuron *81*, 179–194.

Han, X., Chow, B.Y., Zhou, H., Klapoetke, N.C., Chuong, A., Rajimehr, R., Yang, A., Baratta, M. V., Winkle, J., Desimone, R., et al. (2011). A High-Light Sensitivity Optical Neural Silencer: Development and Application to Optogenetic Control of Non-Human Primate Cortex. Front. Syst. Neurosci. *5*, 18.

Harris, J.A., Hirokawa, K.E., Sorensen, S.A., Gu, H., Mills, M., Ng, L.L., Bohn, P., Mortrud, M., Ouellette, B., Kidney, J., et al. (2014). Anatomical characterization of Cre driver mice for neural circuit mapping and manipulation. Front. Neural Circuits *8*, 1–16.

Harvey, C.D., Coen, P., and Tank, D.W. (2012). Choice-specific sequences in parietal cortex during a virtual-navigation decision task. Nature *484*, 62–68.

Jeong, H., Choi, I., Jeong, D., Kim, K., Lee, S., Song, Y., Kim, J., Jeong, H., Choi, I., Jeong, D., et al. (2017). A neural circuit for auditory dominance over visual perception. Neuron *93*, 940–954.e6.

Kamigaki, T., and Dan, Y. (2017). Delay activity of specific prefrontal interneuron subtypes modulates memory-guided behavior. Nat. Neurosci. *20*, 854–863.

van Kerkoerle, T., Self, M.W., and Roelfsema, P.R. (2014). Effects of attention and working

memory in the different layers of monkey primary visual cortex. Soc.Neurosci.Abstr. *8*, 263.13.

Kiritani, T., Galan, K., Sreenivasan, V., Esmaeili, V., Kiritani, T., Galan, K., Crochet, S., and Petersen, C.C.H. (2016). Movement Initiation Signals. Neuron *92*, 1368–1382.

Knutsen, P.M., Derdikman, D., Ahissar, E., Magne, P., Derdikman, D., and Track-, E.A. (2005). Tracking Whisker and Head Movements in Unrestrained Behaving Rodents. 2294–2301.

Knutsen, P.M., Pietr, M., and Ahissar, E. (2006). Haptic Object Localization in the Vibrissal System: Behavior and Performance. J. Neurosci. *26*, 8451–8464.

Kwon, S.E., Yang, H., Minamisawa, G., and O'Connor, D.H. (2016). Sensory and decision-related activity propagate in a cortical feedback loop during touch perception. Nat. Neurosci. *19*, 1243–1249.

Langer, D., van 't Hoff, M., Keller, A.J., Nagaraja, C., Pfäffli, O.A., Göldi, M., Kasper, H., and Helmchen, F. (2013). HelioScan: A software framework for controlling in vivo microscopy setups with high hardware flexibility, functional diversity and extendibility. J. Neurosci. Methods *215*, 38–52.

Leavitt, M.L., Mendoza-Halliday, D., and Martinez-Trujillo, J.C. (2017). Sustained Activity Encoding Working Memories: Not Fully Distributed. Trends Neurosci. *40*, 328–346.

Lein, E.S., Hawrylycz, M.J., Ao, N., Ayres, M., Bensinger, A., Bernard, A., Boe, A.F., Boguski, M.S., Brockway, K.S., Byrnes, E.J., et al. (2007). Genome-wide atlas of gene expression in the adult mouse brain. Nature *445*, 168–176.

Li, N., Chen, T.-W., Guo, Z. V., Gerfen, C.R., and Svoboda, K. (2015). A motor cortex circuit for motor planning and movement. Nature *519*, 51–56.

Licata, A.M., Kaufman, M.T., Raposo, D., Ryan, M.B., Sheppard, J.P., and Churchland, A.K. (2017). Posterior parietal cortex guides visual decisions in rats. J. Neurosci. *37*, 0105–0117.

Liu, D., Gu, X., Zhu, J., Zhang, X., Han, Z., Yan, W., Cheng, Q., Hao, J., Fan, H., Hou, R., et al. (2014). Medial prefrontal activity during delay period contributes to learning of a working memory task. Science (80-.). *346*, 458–463.

Ma, Y., Shaik, M.A.M., Kim, S.H., Kozberg, M.G.M., Zhao, H.T.H., Yu, H., Hillman, E.M.C.E., Thibodeaux, D.N., Zhao, H.T.H., Yu, H., et al. (2016). High-speed, wide-field optical mapping (WFOM) of neural activity and brain haemodynamics: Considerations and novel approaches. Philos Trans R Soc L. B Biol Sci. *371*, 20150360.

Madisen, L., Garner, A.R., Shimaoka, D., Chuong, A.S., Klapoetke, N.C., Li, L., van der Bourg, A., Niino, Y., Egolf, L., Monetti, C., et al. (2015). Transgenic mice for intersectional targeting of neural sensors and effectors with high specificity and performance. Neuron *85*, 942–958.

Makino, H., Ren, C., Liu, H., Kim, A.N., Kondapaneni, N., Liu, X., Kuzum, D., and Komiyama, T. (2017). Transformation of Cortex-wide Emergent Properties during Motor Learning. Neuron *94*, 880–890.e8.

Manita, S., Suzuki, T., Homma, C., Matsumoto, T., Odagawa, M., Yamada, K., Ota, K., Matsubara, C., Inutsuka, A., Sato, M., et al. (2015). A Top-Down Cortical Circuit for Accurate Sensory Perception. Neuron *86*, 1304–1316.

Maravall, M., and Diamond, M.E. (2015). Functional principles of whisker-mediated touch perception. Sensorimotor Integr. Whisker Syst. *25*, 169–193.

Marcos, A.S., and Harvey, C.D. (2016). History-dependent variability in population dynamics during evidence accumulation in cortex. Nat. Neurosci. *19*, 1672–1680.

Mayford, M., Bach, M.E., Huang, Y.-Y., Wang, L., Hawkins, R.D., and Kandel, E.R. (1996). Control of Memory Formation Through Regulated Expression of a CaMKII Transgene. Science (80-.). *274*, 1678–1683.

Miyashita, T., and Feldman, D.E. (2013). Behavioral detection of passive whisker stimuli requires somatosensory cortex. Cereb. Cortex *23*, 1655–1662.

Mohajerani, M.H., Chan, A.W., Mohsenvand, M., LeDue, J., Liu, R., McVea, D.A., Boyd, J.D., Wang, Y.T., Reimers, M., and Murphy, T.H. (2013). Spontaneous cortical activity alternates between motifs defined by regional axonal projections. Nat. Neurosci. *16*, 1426–1435.

Morita, T., Kang, H., Wolfe, J., Jadhav, S.P., and Feldman, D.E. (2011). Psychometric curve and behavioral strategies for whisker-based texture discrimination in rats. PLoS One *6*.

Murakami, M., Shteingart, H., Loewenstein, Y., and Mainen, Z.F. (2016). Distinct sources of deterministic and stochastic components of action timing decisions in rodent frontal cortex. Neuron *94*, 908–919.e7.

Oh, S.W., Harris, J.A., Ng, L., Winslow, B., Cain, N., Mihalas, S., Wang, Q., Lau, C., Kuan, L., Henry, A.M., et al. (2014). A mesoscale connectome of the mouse brain. Nature *508*, 207–214.

Otchy, T.M., Wolff, S.B.E., Rhee, J.Y., Pehlevan, C., Kawai, R., Kempf, A., Gobes, S.M.H., and Ölveczky, B.P. (2015). Acute off-target effects of neural circuit manipulations. Nature *528*, 358–363.

Platt, M.L., and Huettel, S.A. (2008). Risky business: the neuroeconomics of decision making under uncertainty. Nat. Neurosci. *11*, 398–403.

Poort, J., Khan, A.G., Pachitariu, M., Nemri, A., Orsolic, I., Krupic, J., Bauza, M., Sahani,

M., Keller, G.B., Mrsic-Flogel, T.D., et al. (2015). Learning Enhances Sensory and Multiple Non-sensory Representations in Primary Visual Cortex. Neuron *86*, 1478–1490.

Raposo, D., Kaufman, M.T., and Churchland, A.K. (2014). A category-free neural population supports evolving demands during decision-making. Nat. Neurosci. *17*, 1784–1792.

Roelfsema, P.R., Tolboom, M., and Khayat, P.S. (2007). Different processing phases for features, figures, and selective attention in the primary visual cortex. Neuron *56*, 785–792.

Romo, R., and de Lafuente, V. (2013). Conversion of sensory signals into perceptual decisions. Prog. Neurobiol. *103*, 41–75.

Schneider, D.M., Nelson, A., and Mooney, R. (2014). A synaptic and circuit basis for corollary discharge in the auditory cortex. Nature *513*, 189–194.

Siegel, M., Buschman, T.J., and Miller, E.K. (2015). Cortical information flow during flexible sensorimotor decisions. Science (80-.). *348*, 1352–1355.

Silasi, G., Xiao, D., Vanni, M.P., Chen, A.C.N., and Murphy, T.H. (2016). Intact skull chronic windows for mesoscopic wide-field imaging in awake mice. J. Neurosci. Methods *267*, 141–149.

Siniscalchi, M.J., Phoumthipphavong, V., Ali, F., Lozano, M., and Kwan, A.C. (2016). Fast and slow transitions in frontal ensemble activity during flexible sensorimotor behavior. Nat. Neurosci. *19*, 1–11.

Stüttgen, M.C., and Schwarz, C. (2008). Psychophysical and neurometric detection performance under stimulus uncertainty. Nat. Neurosci. *11*, 1091–1099.

Vanni, M.P., and Murphy, T.H. (2014). Mesoscale Transcranial Spontaneous Activity Mapping in GCaMP3 Transgenic Mice Reveals Extensive Reciprocal Connections between

Areas of Somatomotor Cortex. J. Neurosci. *34*, 15931–15946.

Venkatraman, V., Payne, J.W., Bettman, J.R., Luce, M.F., and Huettel, S.A. (2009). Separate Neural Mechanisms Underlie Choices and Strategic Preferences in Risky Decision Making. Neuron *62*, 593–602.

Wang, Q., and Burkhalter, A. (2007). Area map of mouse visual cortex. J. Comp. Neurol. *502*, 339–357.

Wang, Q., Sporns, O., and Burkhalter, A. (2012). Network Analysis of Corticocortical Connections Reveals Ventral and Dorsal Processing Streams in Mouse Visual Cortex. J. Neurosci. *32*, 4386–4399.

Wekselblatt, J.B., Flister, E.D., Piscopo, D.M., and Niell, C.M. (2016). Large-scale imaging of cortical dynamics during sensory perception and behavior. J. Neurophysiol. jn.01056.2015.

Yang, H., Kwon, S.E., Severson, K.S., and O'Connor, D.H. (2015). Origins of choice-related activity in mouse somatosensory cortex. Nat. Neurosci. *19*, 127–134.

Zhang, S., Xu, M., Kamigaki, T., Hoang Do, J.P., Chang, W.-C., Jenvay, S., Miyamichi, K., Luo, L., and Dan, Y. (2014). Long-range and local circuits for top-down modulation of visual cortex processing. Science (80-.). *345*, 660–665.

Zhao, S., Ting, J.T., Atallah, H.E., Qiu, L., Tan, J., Gloss, B., Augustine, G.J., Deisseroth, K., Luo, M., Graybiel, A.M., et al. (2011). Cell type–specific channelrhodopsin-2 transgenic mice for optogenetic dissection of neural circuitry function. Nat. Methods *8*, 745–752.

Zhuang, J., Ng, L., Williams, D., Valley, M., Li, Y., Garrett, M., and Waters, J. (2017). An extended retinotopic map of mouse cortex. Elife *6*, 1–29.

STAR METHODS

KEY RESOURCES TABLE

CONTACT FOR REAGENT AND RESOURCE SHARING

Further information and requests for resources and reagents should be directed to and will be fulfilled by the Lead Contact, Fritjof Helmchen, helmchen@hifo.uzh.ch

EXPERIMENTAL MODEL AND SUBJECT DETAILS

STAR Methods were carried out according to the guidelines of the Veterinary Office of Switzerland and following approval by the Cantonal Veterinary Office in Zurich.

Animals and surgical procedures. A total of 30 adult male mice (1-9 months old) were used in this study. We used 23 triple transgenic Rasgrf2-2A-dCre;CamK2a-tTA;TITL-GCaMP6f animals, expressing GCaMP6f in excitatory neocortical layer 2/3 neurons (Figure 2A). To generate triple transgenic animals, double transgenic mice carrying CamK2a-Tta (Mayford et al., 1996) and TITL-GCaMP6f (Madisen et al., 2015) were crossed with a Rasgrf2-2A-dCre line (Harris et al., 2014; individual lines are available from The Jackson Laboratory as JAX# 016198, JAX#024103, and JAX# 022864, respectively). The Rasgrf2-2A-dCre;CamK2a-tTA;TITL-GCaMP6f line contains a tet-off system, by which transgene expression can be suppressed upon doxycycline treatment (Garner et al., 2012; Gossen and Bujard, 1992). However, doxycycline treatment is not necessary in these animals, since the Rasgrf2-2A-dCre line holds an inducible system of its own, given that the destabilized Cre (dCre) expressed under the control of the Rasgrf2-2A promoter needs to be stabilized by trimethoprim (TMP) to be fully functional. TMP (Sigma T7883) was reconstituted in Dimethyl sulfoxide (DMSO, Sigma 34869) at a saturation level of 100 mg/ml, freshly prepared for each experiment. For TMP induction, mice were given a single intraperitoneal injection (150 µg TMP/g body weight; 29g needle), diluted in 0.9% saline solution. 8 triple transgenic mice were trained in the texture discrimination task, 3 were trained in a control task without discrimination, 5 were

used for controls (see below), 6 were trained and used for optogenetic experiments (further injected with AAV2.5-CAG-ArchT-GFP; see below), and one was trained on the task and used for retinotopic mapping (m15; Figure S6B). In addition, 2 wild-type mice were trained on the task and used for controls. One Rasgrf2-2A-dCre;CamK2a-tTA;TITL-GCaMP6f mouse was injected with a cre-dependent virus expressing eGFP (AAV2.9.Syn.DIO.EGFP) in the S1BC, M2 and P areas and was trained on the control task. Finally 4 transgenic VGAT-ChR2-EYFP were trained and used for additional optogenetic experiments.

We used an intact skull preparation (Silasi et al., 2016) for chronic wide-field calcium imaging of neocortical activity over several months. Mice were anesthetized with 2% isoflurane (in pure O_2) and body temperature was maintained at 37°C. We applied local analgesia (lidocaine 1%), exposed and cleaned the skull, and removed some muscles to access the entire dorsal surface of the left hemisphere (Figure 2A; ~6 x 8 mm^2; from ~3 mm anterior to bregma to ~1 mm posterior to lambda; from the midline to at least 5 mm laterally). We built a wall around the hemisphere with adhesive material (iBond; UV-cured) and dental cement "worms" (Charisma). Then, we applied transparent dental cement homogenously over the imaging field (Tetric EvoFlow T1). Finally, a metal post for head fixation was glued on the back of the right hemisphere. This minimally invasive preparation enabled high-quality chronic imaging with high success rate. In five mice an additional craniotomy was performed at a later stage to enable cellular resolution two-photon imaging in targeted areas. 3-4 mm diameter glass windows were chronically implanted above either frontal or posterior areas as previously described (Chen et al., 2013; Figure 5A; see below).

METHOD DETAILS

Texture discrimination task with delayed response. Mice were trained on a go/no-go discrimination task with delayed response to separate sensation and action periods and to investigate the short-term memory period (Figure 1A). The behavioral setup has been

described previously (Chen et al., 2013). Each trial started with an auditory cue (2 beeps at 2 kHz, 100-ms duration with 50-ms interval), signaling the approach of either two types of sandpapers (grit size P100: rough texture; P1200: smooth texture) to the mouse's whiskers as 'go' or 'no-go' textures (pseudo-randomly presented with no more than 3 repetitions). The texture stayed in touch with the whiskers for 2 seconds, after which it was moved out. A delay of several seconds (1.2 - 4.5 s) was introduced until an additional auditory cue (response cue; 4 beeps at 4 kHz, 50-ms duration with 25-ms interval) signaled the start of a 2 second response period. A water reward was given to the mouse for licking for the go texture only after the response cue ('hit'). Punishment with white noise was given for licking for the no-go texture ('false alarms'; FA) or licking before the response cue ('early licks'). Reward and punishment were omitted when mice withheld licking for the no-go ('correct-rejections', CR) or go ('Misses') textures. The licking detector remained in a fixed and reachable position throughout the entire trial (Videos S1-4).

Training and performance. Five mice were trained to lick for the P100 texture and 3 mice were trained to lick for the P1200 texture. Mice were first handled and accustomed to head fixation before starting water scheduling. Then, mice were shortly trained to lick for a water reward. Next, mice were presented with the 'go' texture and after reliable licking the 'no-go' texture was gradually introduced (Guo et al., 2014). Only after mice reached high and stable discrimination power (>80% for both Hit and CR trials; typically after around a week), they were confronted with the delay period. We then gradually increased the delay duration according to the mouse's ability (Figure 1B). After extensive training (Training time 6.94 ± 0.82 weeks), mice were able to reliably wait for the response cue while maintaining high performance (Figure S1A; range of delay duration during imaging sessions 1.2-4.5 s). Additional training time was given to mice in order to remain quiet for most of the delay period. These quiet periods enabled to reliably evaluate neocortical activity during the delay, avoiding possible confounding effects of preparatory movements (see also Data Analysis

below). Delay duration was varied between imaging sessions. Performance was quantified as d-prime (Chen et al., 2013): d' = Z(Hit/(Hit+Miss)) – Z(FA/(FA+CR)) where Z denotes the inverse of the cumulative distribution function. Imaging began when mice had stabilized on an expert level (d' > 1.5) with a relatively low percentage of early licks (Figure 1B, C).

Control task. To control the effects of each texture on population responses we trained 3 extra mice on a similar task but with no discrimination (Figure S4). Mice were presented with two textures (i.e. P100 or P1200), and then had to wait for several seconds until a response cue signaled the start of a 2 second response period. A water reward was given to the mouse for licking for both texture types. Similar to the texture discrimination task with delayed response, mice were punished for early licks. Training procedure was kept similar to the texture discrimination delayed task and lasted for around 2-3 weeks.

Wide-field calcium imaging. We used a wide-field approach to image large parts of the dorsal cortex while mice performed the task. A sensitive CMOS camera (Hamamatsu Orca Flash 4.0) was mounted on top of a dual objective setup. Two objectives (Navitar; top objective: D-5095, 50 mm f0.95; bottom objective inverted: D-2595, 25 mm f0.95) were interfaced with a dichroic (510 nm; AHF; Beamsplitter T510LPXRXT) filter cube (Thorlabs). This combination allowed a ~9 mm field-of-view, covering most of the dorsal cortex of the hemisphere contralateral to texture presentation. Blue LED light (Thorlabs; M470L3) was guided through an excitation filter (480/40 nm BrightLine HC), a diffuser, collimated, reflected from the dichroic mirror, and focused through the bottom objective approximately 100 µm below the blood vessels. Green light emitted from the preparation passed through both objectives and an emission filter (514/30 nm BrightLine HC) before reaching the camera. The total power of blue light on the preparation was <5 mW, i.e., <0.1 mW/mm^2. At this illumination power we did not observe any photo-bleaching. Data was collected with a temporal resolution of 20 Hz and a spatial resolution of 512x512 or 2048x2048 pixels. On

each imaging day a green reflectance image was taken as reference to enable registration across different imaging days using the blood vessel pattern (fiber-coupled LED illuminated from the side; Thorlabs).

Mapping and area selection. Each mouse underwent a mapping session under anesthesia (1% isoflurane), in which we presented five different sensory stimuli (contra-lateral side): a moving bar stimulating multiple whiskers, the forelimb paw, or the hindlimb paw (20 Hz for 2 s); visual stimulation with a blue LED in front of the eye (100 ms duration; approximately zero elevation and azimuth); and white noise auditory stimulation (2 s. duration). The averaged evoked maps clearly showed activation patches in the expected areas (Figure 2A; Figure S2A), which were used to define the general borders of sensory areas. Of particular interest were 3 cortical borders: (1) the whisker related S1BC and S2 border (Figure 2B), (2) the cortical space between S1BC and visual cortex which we used to define RL (Figure 2B), (3) the posterior and lateral border of the visual cortex (Vis) where beyond it the posterior area P was defined (Figure S7). These general borders were registered from the mapping day to each imaging day using the reference green images. Within these general borders, and in addition based on stereotaxic coordinates, we manually assigned activation patches for each area in each imaging day. We defined 11 areas: S1BC, S2, RL (2.55 posterior and 3.35 mm lateral from bregma), Vis, Au (auditory areas), P (4.51 posterior and 3.75 mm lateral from bregma; average coordinate of 7 passive mice; Figure S7), S1FL, S1HL, whisker-related primary motor cortex (M1; 1.5 anterior and 1 mm lateral from bregma, corresponding to the whisker evoked activation patch in M1 from the mapping session), ALM (anterior lateral motor cortex; 2.5 anterior and 1.5 mm lateral from bregma (Li et al., 2015)) and M2 (1.5 anterior and 0.5 mm lateral from bregma). In addition, we registered sensation maps onto a 2D top view mouse brain atlas and found that the activation patch posterior to S1, corresponds best to rostro-lateral cortex (RL). To further delineate the border between primary visual cortex (V1) and P, we performed retinotopic mapping in 2 additional passive

mice trained on the task (Figure S7B; m13 and m15). Mice were anesthetized and presented with 6 verticals and 6 horizontal moving bars (ranging from -43˚ to 43˚ in elevation and -46˚ to 46˚ in azimuth; 15˚ width; 2 cycles per second; 5 degrees per cycle). Next, we calculated the elevation and azimuth maps and derived the sign map for each mouse (Figure S7B; Garrett et al., 2014; Zhuang et al., 2017). V1 typically exhibits negative sign values which were used to mark its lateral and posterior border. In both mice, the posterior patch of activation during the delay was mostly lateral and posterior to V1 and fitting to visual lateral cortex (V2L or Visl). This fits the border between P and visual cortex derived from the blue LED presentation (Figure S7A) or full field stimulus on the screen (Figure S7B). Finally, we divided the left hemisphere into frontal (FC) and posterior (PC) cortices based on stereotaxic coordinates (Figure 4C dashed white line; frontal cortex is defined as M1 and M2 in the mouse brain atlas (Franklin and Paxinos)).

Controls for non-calcium related optical signals. In wide-field imaging, each pixel reports an optical signal integrated over the underlying labeled structures (cell bodies, axons and dendrites). This signal is susceptible to non-calcium related signals, e.g. slow hemodynamic responses, which could affect the observed patterns (Allen et al., 2017; Ma et al., 2016; Vanni and Murphy, 2014; Wekselblatt et al., 2016). We performed a series of controls to account for non-calcium related signals (Figure S3):

1) In a separate experiment, we interleaved the blue excitation wavelength with a green reflectance signal (530 nm; 150-ms blue and 50-ms green illumination; Figure S3E-L). The green reflectance signal corresponds to hemodynamic modulations but not calcium-dependent fluorescence changes and thus can be used to correct for the former (Ma et al., 2016; Wekselblatt et al., 2016). For this, we trained two additional Rasgrf2-2A-dCre;CamK2a-tTA;TITL-GCaMP6f mouse on the texture discrimination task and imaged with interleaved blue and green light. In general, we find that correcting the population

signal with a green reflectance signal did not substantially change the results (Figure S3E-L).

2) To control for autofluorescence signals we trained 2 wild-type mice on the task and obtained wide-field imaging in awake performing animals (Figure S3A-D). In general, fluorescence changes were near zero during the sensation and delay periods.

3) As another additional control, we tested whether higher baseline fluorescence in the green channel (not related to the GcAMP6f molecule) may affect the results. For this we injected a virus expressing eGFP (AAV2.9.Syn.DIO.EGFP) in S1BC, M2 and area P of one additional mouse (Rasgrf2-2A-dCre;CamK2a-tTA;TITL-GCaMP6f), which was trained on the control task (Figure S3M-P). Green fluorescence change was near zero during sensation and slightly decreased during the delay, and thus was significantly different than transgenic mice expressing GCaMP6f and trained on the same task.

4) M2 activation is very close to the midline where the superior sagittal sinus may modulate fluorescence. To control for this, we imaged 2 Rasgrf2-2A-dCre;CamK2a-tTA;TITL-GCaMP6f mice with a cranial window crossing the midline during wakefulness. The superior sagittal sinus is modulated during movement but returns to baseline shortly after (200 ms; Figure S8) and remains at baseline during quiet periods, implying that M2 enhanced fluorescence during the delay (taken only on quiet periods and lasting for several seconds) is not likely to be affected.

5) In 5 out of the 8 trained mice we implanted a cranial window and imaged single cells in behavioral relevant areas (Figure 5). Cellular-resolution imaging confirmed the results indicating a direct relationship between the wide-field population signal and cell bodies in layer 2/3 (see relevant section in the Results).

In summary, the results from all the above control experiments indicate no major influence of non-calcium-related intrinsic signals on the GCaMP6f signals that would confound our signal interpretations.

Whisker and body tracking. In addition to wide-field imaging, we tracked movements of the whiskers and the body of the mouse during the task (Figure 1A). The mouse was illuminated with a 940-nm infra-red LED. Whiskers were imaged at 200 Hz (500x500 pixels) using a high-speed CMOS camera (A504k; Basler), from which we calculated time course of whisking envelope and the time of first touch (see below). An additional camera monitored the movements of the mouse at 30 Hz (The imaging source; DMK 22BUC03; 720x480 pixels). We used movements of both forelimbs and the head/neck region to assess body movements, to reliably detected large movements and enabled labeling trials as active or passive (Figure S6A; see *Data Analysis* below and Videos S1-4).

Two-photon calcium imaging. In five mice, we made additional craniotomies over cortical areas of interest based on wide-field imaging. For mouse #3, #4 and #6 we positioned a 3-mm glass window over M2; for mouse #5 and #8 we positioned a 4-mm glass window over the posterior sensory areas, covering S1BC, S2, RL, and P areas (Figure 5A). Mice were given a week to recover from surgery and were re-trained for an additional week before two-photon imaging began. We used a custom-built two-photon microscope controlled by HelioScan (Langer et al., 2013), equipped with a Ti:sapphire laser system (Mai Tai HP; Newport Spectra Physics), a water-immersion objective (Olympus 340LUMPlanFl/IR, NA 0.8), galvanometric scan mirrors (model 6210; Cambridge Technology), and a Pockel's Cell (Conoptics) for laser intensity modulation. Based on previous wide-field imaging, along with the blood vessel pattern, we targeted specific areas of interest for two-photon imaging of L2/3 neurons in each

mouse. We excited GCaMP6f at 940 nm and detected green fluorescence with a photomultiplier tube (Hamamatsu). Images (128x64 pixels) were acquired at 12-Hz frame rate and 10-50 cells per field of view were imaged simultaneously.

Optogenetic experiments. To study whether M2 and P areas are behaviorally relevant, we trained a second batch of mice expressing GCaMP6f in layer 2/3 excitatory neurons (Figure 6A; n = 6; mice #9-14). Each mouse was investigated using wide-field imaging, labelled as active or passive according to its main strategy, and the relevant activation patches during the delay period in M2 and P, respectively, were found (Figure 6B). Next, mice were anesthetized, a small craniotomy was made through the intact skull preparation, and an AAV2.5-CAG-ArchT-GFP injection was targeted to M2 for active mice and P for passive (420–nl volume targeting the entire cortical column). Next, the hole was covered with clear dental cement and after 4-5 weeks perturbation experiments began. A 400-µm optical fiber was placed over the relevant area for illumination with green laser light (561 nm; 14-29 mW; CW laser Coherent OBIS-561-50 LS). Light was randomly delivered in 50% of the trials during the delay period (n=17, 19, 19, 24, 16 and 12 perturbation sessions from mice #9-14 respectively). In some sessions light was delivered during both sensation and delay periods. In addition, in a minority of session we delivered light only in 10% of the trials. Results were similar in all of the above cases and were pooled together.

In addition, we trained 4 transgenic VGAT-ChR2-EYFP mice expressing channelrhodopsin-2 in GABAergic inhibitory neurons across the whole cortex (Zhao et al., 2011; strain 14548; Jackson lab). These mice underwent the same wide-field preparation and were used to silence both P and M2 using two optical fibers (910 µm) that were coupled with blue laser light during the delay period (450 nm; 40 Hz; 7-11 mW each fiber; Coherent BioRay-450nm-50mw). Coordinates of M2 and P were determined based on the activation patches obtained from the previous mice (for P area: 4.51 posterior and 3.75 mm lateral from

bregma; for M2 area: 1 anterior and 0.5 mm lateral from bregma). Light was delivered on 10-50% of the trials randomly only during the delay period (n = 11, 19, 10 and 15 optogenetic recording sessions from VGAT mice 1-4 respectively).

Controls for optogenetic experiments. In all mice with ArchT injections there was clear additional green fluorescence from the GFP tag around the injection site visualized both through the wide-field preparation and with post-hoc histology. To validate the opsin, we injected AAV-CAG-ArchT-GFP into S1BC in one Rasgrf2-2A-dCre;CamK2a-tTA;TITL-GCaMP6f mouse. Next, a small craniotomy was made and a 16-channel silicon probe was inserted into S1BC. Green light was coupled through a fiber (maintaining the same parameters of the optogenetic experiments) on interleaved trials both during whisker stimulation and spontaneous activity. In both cases, light stimulation caused a significant initial hyperpolarization peak in the local field potential indicating that the local neuronal population is perturbed with an inhibitory component ($P < 0.05$; Mann-Whitney U test between light and no light trials; n = 100 and 90 trials for spontaneous and stimulus evoked conditions).

To control for the light disturbance we performed four different experiments: 1) In the same ArchT mice that underwent the optogenetic experiments, we delivered light in other parts of the cortex not expressing ArchT. Performance between light and no-light trials was not significantly different ($P > 0.05$; Singed rank test for 5 different mice separately). 2) Green light with similar parameters as in the optogenetic experiments was delivered on trained mice with a wide-field preparation that were not injected with the virus showing no significant change in performance ($P > 0.05$; Singed rank test for 2 different mice separately). 3) In the VGAT mice, we photo-inhibited only during the sensation period (from -1 to 2 seconds relative to texture stop; same position and parameters as optogenetic experiments) resulting in no significant change in performance ($P > 0.05$; Singed rank test for 2 different mice separately). 4) VGAT mice performed the task with similar illumination as in the

optogenetic experiments but with light blocked by covering the wide-field preparation with black aluminum foil. There was no significant change in performance ($P > 0.05$; Singed rank test for 2 different mice separately). In summary, these control experiments demonstrate that light delivered above the wide-field preparation alone does not affect the performance of the mice but that it needs to reach the relevant neuronal populations at the right time to become effective.

QUANTIFICATION AND STATISTICAL ANALYSIS

Data analysis. Data analysis was performed using Matlab software (Mathworks). A high number of imaging sessions and trials per session enabled statistical analysis within each mouse (24.6 ± 4.5 imaging sessions; 105 ± 5 trials per session; n = 8 mice; mean ± s.e.m). Wide-field fluorescence images were sampled down to 256x256 pixels and pixels outside the imaging area were discarded. Each pixel and each trial were normalized to baseline several frames before the first auditory cue (frame 0 division). To study neural dynamics during sensation, we used a different baseline, several frames before the first touch of the whiskers on the texture (Figure 2; see also ***Whisker tracking and first-touch analysis*** below). Next, trials were divided into 5 categories: Hit, CR, FA, Miss and Early lick. Since imaging was performed on expert mice, we mainly focused mainly on correct trials, i.e. hit and CR trials (but see Figure 8 for error analysis).

Trial classification based on the body movements. We used a body camera to detect general movements of the mouse (30 Hz frame rate; Figure 1A). In general, when mice moved during the trial, specifically during the texture approach, they typically moved their forelimbs along the support pole, arched their back and actively whisked (Videos S1-4). For each recording day, we first outlined the forelimbs and the neck areas (one area of interest for each), which were reliable areas to detect general movements. Next, we calculated the body movement (1 minus frame-to-frame correlation) within these areas as a function of time for

each trial (Figure 1D). Thresholding at 3 s.d. above baseline (defined as the 5th percentile) resulted in a binary movement vector (either 'moving' or 'quiet') for each trial (Figure 1D). Binary movement vectors were validated manually from the body camera for representative imaging sessions. A trial was labeled (unrelated to hit or CR) as 'active' if the mouse was moving for at least 0.5 seconds during the sensation period (-1 s to 2 s relative to texture stop) and 'passive' otherwise. Different movement thresholds or minimal duration criteria yielded similar results. 'Activeness' was defined as the percentage of active hit trials and derived for each imaging session (Figure 1F; Figure S1B for movement probabilities during the sensation and delay periods for each mouse). To analyze the delay period, we focused only on quiet trials where the mouse did not move for at least the first second in the delay (starting 0.2 s after beginning of texture retraction; Figure 3A). Trials where the mouse moved during the first second of the delay period where defined as noisy and discarded from the analysis (Figure 1D; bottom trace). For the remaining trials, we detected the first frame where the mouse moved after 1 s into the delay and truncated the $\Delta F/F$ traces after this point (Figure S6A, B). Therefore, the data analysis for the delay period excluded any movement-related activity and reflects the population dynamics when the mouse is sitting quietly and maintaining information to guide its future action. In a small subset of sessions where the body camera videos were of low quality or the camera was missing, we labeled trials based on the population dynamics in the cortex. M2 and somatosensory forelimb cortex (S1FL) were found to be the areas most predictive of the mouse's movements. By thresholding the M2 and S1FL for movement onset and offset we reconstructed the movement vectors for each trial and were able to accurately classify trial labels (active or passive; 80% accuracy). Finally, as an alternative we defined activeness based on whisking envelope (threshold of 2˚ from -1 to 0 s relative to texture stop), yielding similar trial classification as for considering body movements (86.5 ± 8.7% overlap; mean ± std from 69 imaging sessions) and with our main results unchanged.

Whisker tracking and first-touch analysis. The average whisker angle across all imaged whiskers was measured using automated whisker tracking software (Knutsen et al., 2005). The mean whisker envelope was calculated as the difference between maximum and minimum whisker angles along a sliding window equal to the imaging frame duration (50 ms; Chen et al., 2013). In addition, we manually detected the first frame, in which any whisker touched the upcoming texture, using the movies from the whisker cameras (Figure 1H; LabVIEW custom program). The first touch occurred on average 0.47 s before the texture stopped (ranging from 0.1-1.1 s). Time of first touch did not differ between hit and CR trials ($P > 0.05$; Mann-Whitney U-test for each mouse separately). Due to the large range of the first touch times, to study the sensation part we aligned the population signal of each trial to the corresponding first touch and normalized to baseline just before the first touch (Figures 2 and 5B, C).

SVM classification of hit vs. CR for different trial types. To study how well the population signal can predict the upcoming choice (i.e. hit or CR) and which pixels are most informative, we trained (80% of the trials) a linear support vector machine (SVM) to classify trials into hit or CR (test on the remaining 20%; Figure 4). The input to the SVM were the delay maps (each pixel was considered as a feature) separated into active trials (hit vs. CR trials) or passive trials (hit vs. CR trials). The SVM was performed for each recording day (n = 4, 2, 8, 9, 10, 9, 7 and 12 recording days for mice 1-8, respectively), with 20 cross validations, after which accuracy and weights (i.e. coordinates of an orthogonal vector to the separating hyperplane) were averaged across iterations. A minimum of 15 trials was needed to run the SVM. Due to limited trial numbers SVM was performed on active trials only for mice 1, 3, 5, and 6 and for passive trials only for mice 2, 4, 6, 7 and 8 (Figure 4B). To reduce noise, we initially performed a principal component analysis (PCA) analysis on the delay maps and each pixel (feature) was represented by the top 25 PCs (explaining 82.9 ± 3.6 and 89.8 ± 1.7 of the variance, for active and passive trials, respectively; mean ± s.e.m). This pre-processing

procedure optimally balanced between high accuracy and good localization. In general, using fewer PCA components resulted in better localization (i.e. pixels were mostly grouped, related to patches of activity and consistent across imaging days) but worse accuracy. Using more components (up to using the raw data) resulted in worse localization (i.e. pixels were less grouped, more randomly distributed and less consistent across imaging days), but better accuracy. To test for significance, we shuffled between hit and CR labels (while maintaining active and passive labels) and performed the same SVM, resulting in an accuracy of 48.5 ± 4.2 and 50.4 ± 3.8 (mean ± s.e.m), i.e. chance level, for active and passive trials, respectively. In an additional analysis, we calculated the discrimination power between hit and CR during the delay for individual areas separately (Figure S5C). We calculated a receiver operating characteristics (ROC) curve for each pixel in a given area and calculated its area under the curve (AUC). This procedure was applied for the active and passive strategy separately similar to the SVM analysis. For each area AUC values were averaged across pixels. Finally, to further test the classification of only a subset of pixels, we performed the SVM based on only frontal or posterior cortex (Figure 4F).

Single-cell analysis from two-photon imaging. Using two-photon imaging we could image single cells in areas derived from the population signal. Calcium image processing was previously described (Chen et al., 2013). In short, green channel images underwent background subtraction, X-Y motion correction, and normalization to baseline fluorescence (calculated from several frames before the stimulus cue similar to the wide-field data). Single cells were outlined manually from the mean image of a single-trial time series. Z-motion correction excluded any frames, in which several focused cells abruptly dropped in fluorescence by 20%. Responsive cells were defined either for the sensation period (for S1BC, S2 and RL cells) or the delay period (M2 and P cells) by crossing a signal-to-noise ratio (SNR) threshold of 1.5. Number of responsive cells in posterior areas for mouse #5/#8: S1BC: 260/168, S2: 129/108, RL: 120/7, P: 23/374. Number of responsive cells in M2 mouse

#3/#4/#6: 27/207/254. Trial were classified based on the mouse's movement as for the wide-field imaging experiments. For a small subset of sessions where the body camera gave low quality images or was missing, we predicted the mouse's movement based on the z-axis drop in focus (using a 10% drop from baseline in 3 in-focus single cells as criterion; 75% accuracy in labeling trials by validating with move vector from the body camera).

Error trials analysis. To investigate what type of information is maintained in areas P and M2 we also analyzed error trials, i.e. FA and Miss trials, and compared them to correct trials, i.e. hit and CR trials. The idea is that if the activity in an area is similar for trial types with the same future action (hit and FA; CR and Miss), then this area is more likely to encode motor-related information. Likewise, if the activity of an area is similar for trial types with the same past stimulus identity (hit and Miss; CR and FA), then this area is more likely to encode sensory-related information. Each error trial was classified as active or passive similar to correct trials. Due to the low number of error trials (6%/5% and 10%/12% fraction of FA/Misses for active and passive trials, respectively; averaged across all mice), all error trials were pooled together from all recording days for each mouse separately. In our study we focused on the activity during the delay period in M2 for active trials and in area P for passive trials. To relate each error type with either its past sensory stimulus or its future motor action, we defined a motor-sensory index. For each error type we calculated its mean activity (averaged during the delay period and across all recording days) during the delay in M2 for active trials and in P for passive trials. This was done for each mouse separately. MSI for FA trials was calculated as follows:

$$\Delta M_{FA} = |R_{FA} - R_{hit}| \tag{1.1}$$

$$\Delta S_{FA} = |R_{FA} - R_{CR}| \tag{1.2}$$

$$MSI_{FA} = \frac{\Delta S_{FA} - \Delta M_{FA}}{\Delta S_{FA} + \Delta M_{FA}} \tag{1.3}$$

where R denotes the mean ΔF/F response during the delay in M2 and P for active and passive trials, respectively. MSI for Miss trials was calculated analogously as:

$$\Delta M_{miss} = |R_{miss} - R_{CR}| \quad (2.1)$$

$$\Delta S_{miss} = |R_{miss} - R_{hit}| \quad (2.2)$$

$$MSI_{miss} = \frac{\Delta S_{miss} - \Delta M_{miss}}{\Delta S_{miss} + \Delta M_{miss}} \quad (2.3)$$

The final MSI for each mouse was calculated as the weighted average (according to trial numbers) of MSI_{FA} and MSI_{Miss}. See also Figure 8C for a schematic illustration. MSI ranges from -1 to 1 where positive values indicate greater encoding of motor-related information (similar activity for similar future action) whereas negative values indicate greater encoding of sensory-related information (similar activity for similar past stimuli).

Statistical analysis. In general, non-parametric two-tailed statistical tests were used, Mann-Whitney U-test to compare between two medians from two populations or the Wilcoxon signed rank test to compare a population's median to zero (or between two paired populations). Due to a relatively large number of imaging sessions from each mouse, we were able to compute within-mouse statistics (Figures 6D-F and 7F; Figures S2C, D, 3D, 3O 6C, 7E). An ANOVA and multiple group correction were used when comparing between more than two groups (Figure 4D-F and Figure S6D). In cases were ANOVA was applied, data was not significantly different from normal distribution ($P > 0.05$; Kolmogorov-Smirnov test on residuals). Post-hoc significant test was done between groups (Tukey-Kramer test) or comparing values of one group against zero (95% confidence intervals different from zero). SVM classification was done with 20 cross-validations and trial label shuffling (see relevant section above).

SUPPLEMENTAL INFORMATION

Inventory of Supplemental Information

This study contains 9 Supplemental Figures and 4 Supplemental Videos.

Figure S1. Related to Figure 1, Additional behavioral results for individual mice.
Figure S2. Related to Figure 2, Mapping sessions, sensation maps and grand averages in different mice.
Figure S3. Related to Figures 2 and 3. Controls for non-calcium related optical signals.
Figure S4. Related to Figure 2, Mice trained on a similar task without discrimination did not show difference in responses between textures.
Figure S5. Related to Figures 2-5. Mean activity and decoding compared across all areas during the sensation and delay periods.
Figure S6. Related to Figure 3. Effects of movements on population responses and discarding movement periods during the delay period.
Figure S7. Related to Figure3. Additional results and controls for the delay period.
Figure S8. Related to Figure 3. Midline area is modulated during movement but returns to baseline shortly after.
Figure S9. Related to Figure 6. Behavioral parameters for ArchT-mediated optogenetic experiments.

Video S1 - Related to Figure 3. Active hit trial in mouse #6.
Video S2 - Related to Figure 3. Passive hit trial in mouse #6.
Video S3 - Related to Figure 3. Active hit trial in mouse #5.
Video S4 - Related to Figure 3. Passive hit trial in mouse #7.

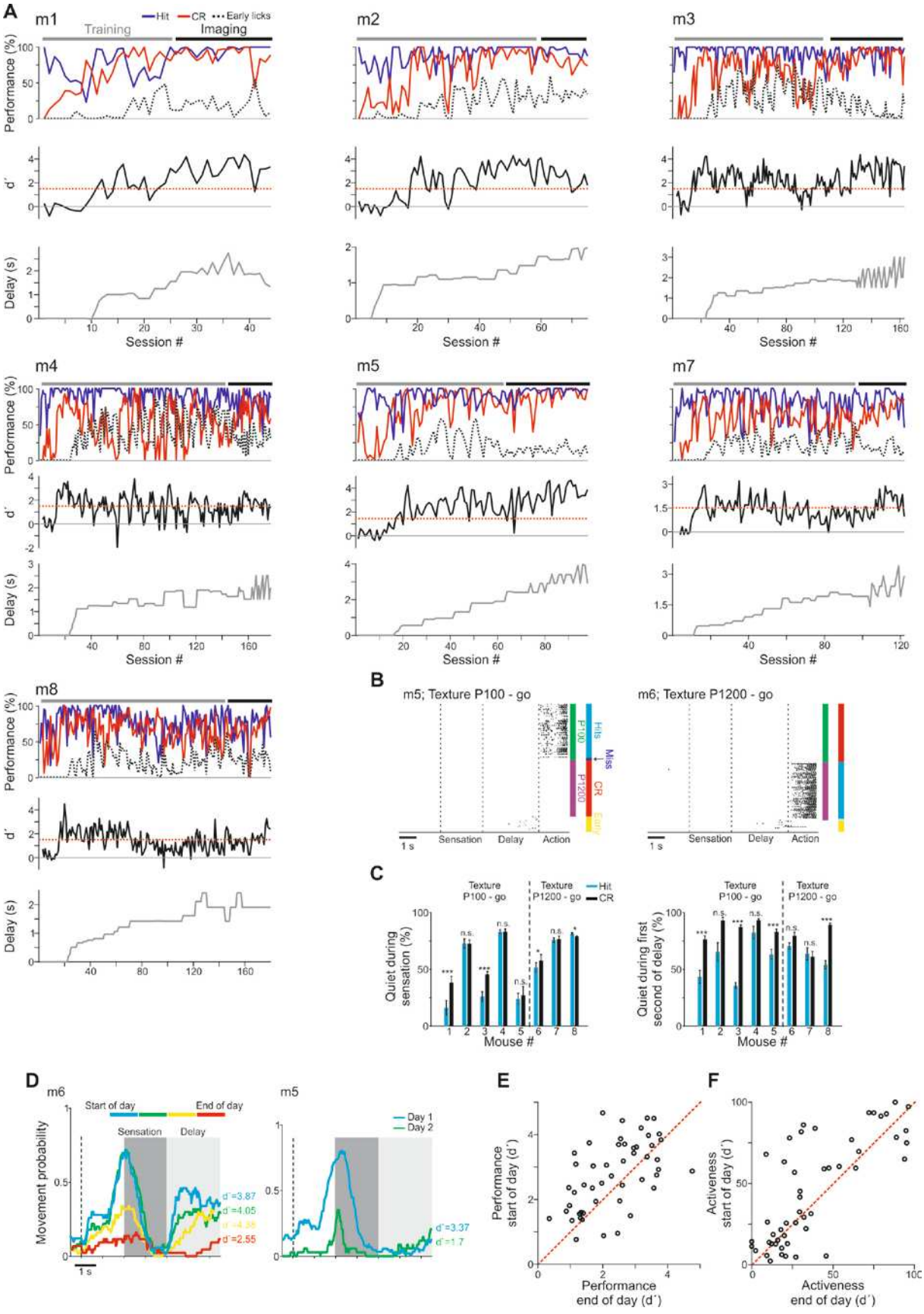

Figure S1. Related to Figure 1, Additional behavioral results for individual mice.

(A) Performance and delay duration throughout training and imaging for the remaining 7 mice (similar to mouse #6 in Figure 1B).

(B) Licking raster plots in an example recording session in two mice. Each row is one trial and each dot is a licking event. Texture types and behavioral outcomes are labeled on the right. Each mouse is trained to lick (go) for a different texture.

(C) Percentage of quietness during the sensation period (left; i.e. mouse moved for less than 0.5 s from -1 to 2 s relative to texture stop) and the delay period (right; mouse did not move during at least the first second of the delay) for each mouse in hit (blue) and CR (black) trials. Error bars are s.e.m. across imaging sessions.

(D) *Left:* Movement probability during a full imaging day for an example mouse (#6). All trial types were included (i.e. active, passive and noisy) without cutting out periods of movements during the delay. This mouse decreased its activeness as the day progresses. *Right:* Movement probability on two different imaging days for another example mouse (#5). This mouse was more active on one day compared to the other.

(E) Comparison of performance (d') between the start and end of each recording day for each mouse (calculated from first and last 100 trials, respectively). Each dot is one recording day.

(F) Comparison of activeness between the start and end of each recording day for each mouse (calculated from first and last 100 trials, respectively). Each dot is one recording day.

* $P < 0.05$. ** $P < 0.01$. *** $P < 0.001$. n.s. not significant. Wilcoxon signed-rank test.

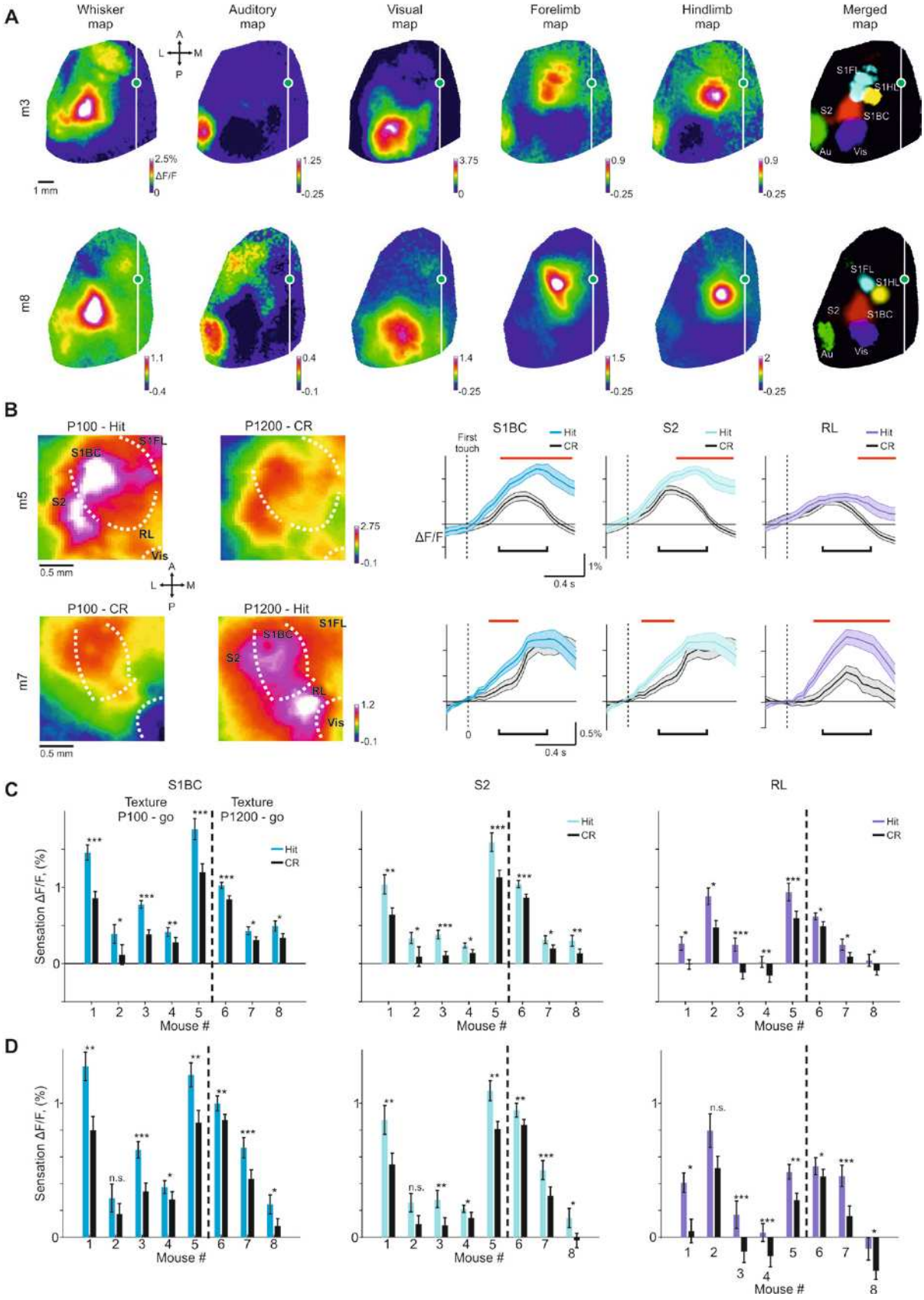
A
Whisker map
Auditory map
Visual map
Forelimb map
Hindlimb map
Merged map
m3
m8
S1FL
S1HL
S2
S1BC
Au
Vis
1 mm
B
P100 - Hit
P1200 - CR
P100 - CR
P1200 - Hit
m5
m7
RL
0.5 mm
S1BC
S2
RL
First touch
Hit
CR
ΔF/F
1%
0.4 s
0.5%
C
Texture P100 - go
Texture P1200 - go
Sensation ΔF/F, (%)
Mouse #
D
n.s.

Figure S2. Related to Figure 2, Mapping sessions, sensation maps and grand averages in different mice.

(A) Each mouse underwent a mapping session including five stimulus modalities: whisker, auditory, visual, forelimb and hindlimb (STAR Methods). Mean activation maps are shown for each stimulus type along with the merged map for two example mice. Color denotes normalized fluorescence ($\Delta F/F$).

(B) Examples of sensation maps (of whisker-related posterior areas) and time courses from two more mice in addition to the mice shown in Figure 2B, C. Each mouse is trained to lick for a different go texture. Red lines indicate time frames with significant difference between hit and CR trials. Black bars indicate time windows for calculation of sensation maps.

(C) Activation during sensation in hit versus CR trials averaged across all trial types (active and passive together) in S1BC, S2 and RL for each mouse separately. Error bars are s.e.m. across imaging sessions.

(D) Similar to c but only for passive trials.

* $P < 0.05$. ** $P < 0.01$. *** $P < 0.001$. n.s. not significant. Wilcoxon signed-rank test.

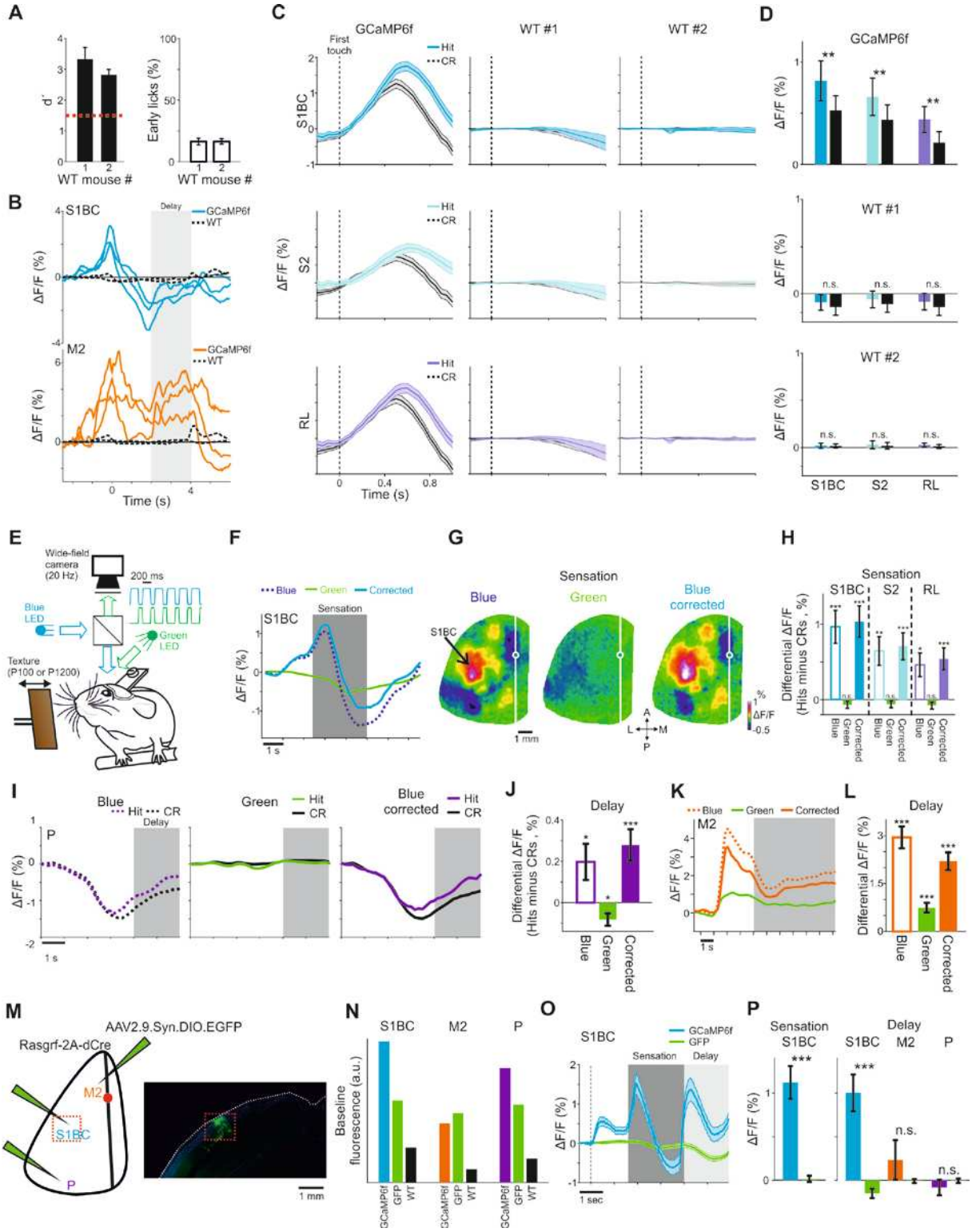
A
d'
Early licks (%)
WT mouse #
WT mouse #
B
S1BC
GCaMP6f
WT
Delay
M2
ΔF/F (%)
Time (s)
C
GCaMP6f
WT #1
WT #2
First touch
Hit
CR
S1BC
S2
RL
Time (s)
D
GCaMP6f
WT #1
WT #2
ΔF/F (%)
n.s.
S1BC
S2
RL
E
Wide-field camera (20 Hz)
200 ms
Blue LED
Green LED
Texture (P100 or P1200)
F
Blue
Green
Corrected
S1BC
Sensation
ΔF/F (%)
1 s
G
Sensation
Blue
Green
Blue corrected
S1BC
1 mm
%
ΔF/F
H
Sensation
S1BC
S2
RL
Differential ΔF/F (Hits minus CRs , %)
Blue
Green
Corrected
I
Blue
Green
Blue corrected
Hit
CR
Delay
P
ΔF/F (%)
1 s
J
Delay
Differential ΔF/F (Hits minus CRs , %)
Blue
Green
Corrected
K
Blue
Green
Corrected
M2
ΔF/F (%)
1 s
L
Delay
Differential ΔF/F (%)
Blue
Green
Corrected
M
AAV2.9.Syn.DIO.EGFP
Rasgrf-2A-dCre
M2
S1BC
P
1 mm
N
S1BC
M2
P
Baseline fluorescence (a.u.)
GCaMP6f
GFP
WT
O
S1BC
GCaMP6f
GFP
Sensation
Delay
ΔF/F (%)
1 sec
P
Sensation
S1BC
Delay
S1BC
M2
P
ΔF/F (%)
n.s.

Figure S3. Related to Figures 2 and 3. Controls for non-calcium related optical signals.

(A-D) Control for auto-fluorescence changes in trained wild-type (WT) mice display near-zero modulation.

(A) Behavioral performance (d') and percentage of early licks in two WT mice trained on the delayed texture discrimination task (similar to Figure 1C). Error bars are s.e.m. over imaging sessions.

(B) Example population response (ΔF/F; averaged across all hit trials) in S1BC (left) and M2 (right) in 3 transgenic mice (expressing GCaMP6f in layer 2/3 of excitatory cells; colored traces) and the two WT mice (black dashed traces). Delay period is highlighted in gray.

(C) Example population response in hit and CR trials aligned to the first touch for an example transgenic mouse and two WT mice (similar to Figure 2C). Error bars are s.e.m. across trials.

(D) Responses during the sensation period in hit and CR trials for the transgenic mice (top; similar to Figure 2D; Error bars are s.e.m across mice) and for the two WT mice (error bars are s.e.m. across imaging sessions; n=11 and 23 imaging sessions for WT #1 and #2 respectively). ** $P < 0.01$. n.s. not significant. Wilcoxon signed-rank test.

(E-L) Control for intrinsic signal changes maintains the results.

(E) Additional two mice were trained on the delayed texture discrimination task (d'=2.54 and 3.6, early licks 25% and 10%; activeness 24% and 85%) for which we imaged the dorsal hemisphere with interleaved blue (475 nm) and green (520 nm) light (150 ms blue and 50 ms green; 50 ms interval between; STAR Methods).

(F) Example population response from S1BC for blue (dashed dark blue), green and corrected blue (blue trace minus the green trace). Sensation period is highlighted in gray.

(G) Example sensation maps (averaged 0.3 to 0.7 s after first touch) for the blue, green and corrected blue signals.

(H) Difference in response (hit minus CR trials) during the sensation period in S1BC, S2 and RL for the blue, green and corrected blue signals. Error bars are s.e.m. across trials (n=39 and 90 trials from hit and CR trials respectively). Responses are significantly higher in hit trials for the three ROIs both before and after correction.

(I) Population responses in the P area (hit versus CR trials) for blue, green and corrected blue signals. Delay period is highlighted in gray.

(J) As in H, but for the P area in the delay period. Responses are higher in hit trials for the three ROIs both before and after correction.

(K) as in F but for M2 in an active mouse.

(L) as in H but for M2. * $P < 0.05$. ** $P < 0.01$. *** $P < 0.001$. n.s. not significant. Wilcoxon signed-rank test.

(M-Q) Control for non-calcium dependent fluorescence changes displays near zero changes.

(M) *Left:* Layer 2/3 Cre mouse was injected with a virus expressing eGFP in S1BC, M2, and P areas (STAR Methods). Next, the mouse was trained on the control task (STAR Methods) *Right:* Confocal image of a coronal slice including S1BC injection site (outlined in red square).

(N) Baseline fluorescence in the three areas for GCaMP6f, GFP and WT mice. Values were obtained under the same illumination conditions.

(O) Example population responses (ΔF/F; averaged across all hit trials in the P100 texture) in S1BC from GCaMP6f and GFP mice during the control task. GFP responses are near zero and tend to decrease during the delay. Error bars are s.e.m. across trials.

(P) Responses during the sensation (left; S1BC) and delay (right; S1BC, M2 and P) periods for GCaMP6f (colored) and GFP (green) mice. Error bars are s.e.m. over imaging sessions (n=13 and 11 imaging sessions for GFP and GCaMP6f mice respectively).

*** $P < 0.001$, n.s. – not significant. Mann Whitney U-test.

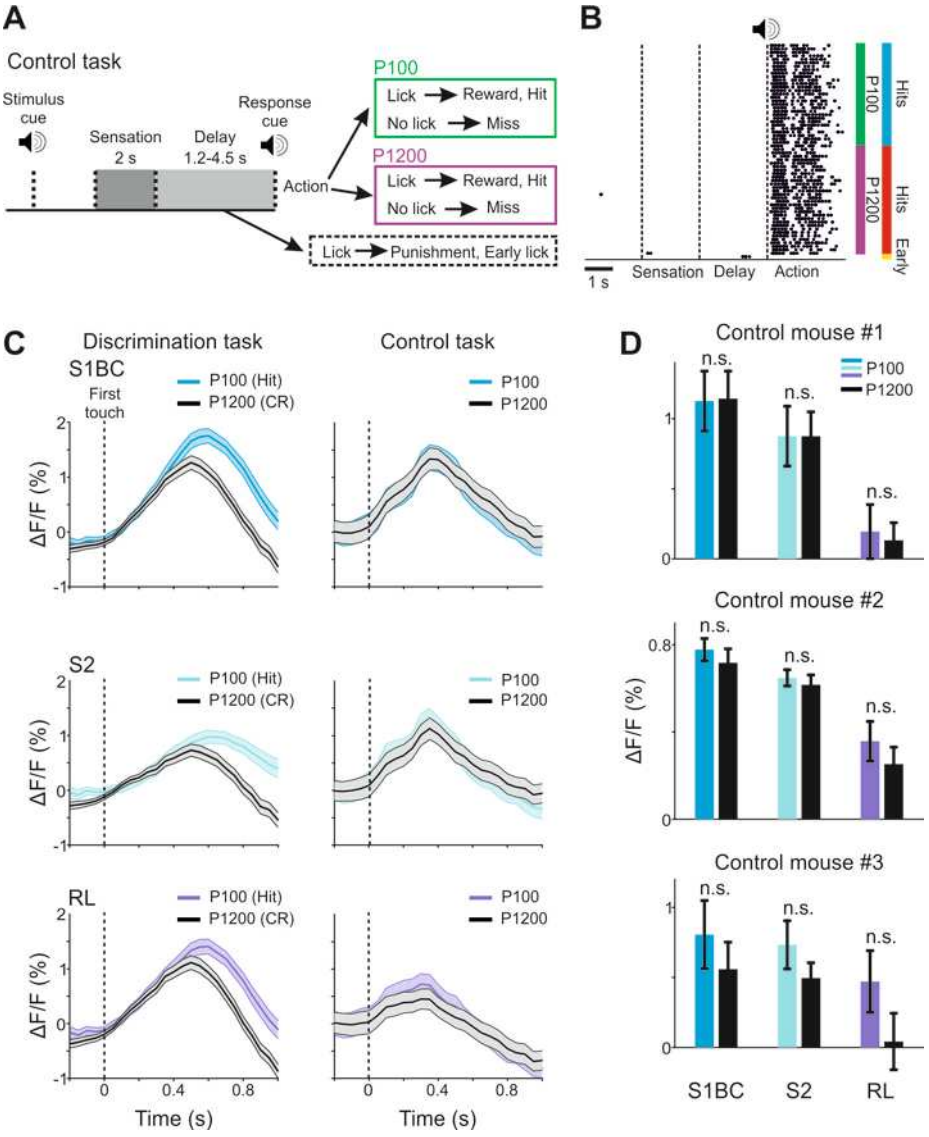

Figure S4. Related to Figure 2. Mice trained on a similar task without discrimination did not show difference in responses between textures.

(A) We trained three mice on a control task resembling the delayed texture discrimination task (Figure 1A). In this task mice received reward for both textures but only if they withheld their response for several seconds until a response cue (STAR Methods).

(B) Licking raster plot in an example recording session. Each row is one trial and each dot is a licking event. Texture types and behavioral outcomes are labeled on the right.

(C) Example population response for the two textures aligned to the first touch (similar to Figure 2C) of a mouse trained on discrimination task (left) and a mouse trained on the control task (right). Error bars are s.e.m. across trials.

(D) Responses during sensation for the two textures (P100 colored and P1200 black) for the three mice trained on the control task. Error bars are s.e.m. across imaging sessions (n = 11, 9 and 12 imaging sessions for control mice #1, #2 and #3 respectively). Responses were slightly biased in favor of the P100 texture. n.s., not significant. Wilcoxon signed-rank test.

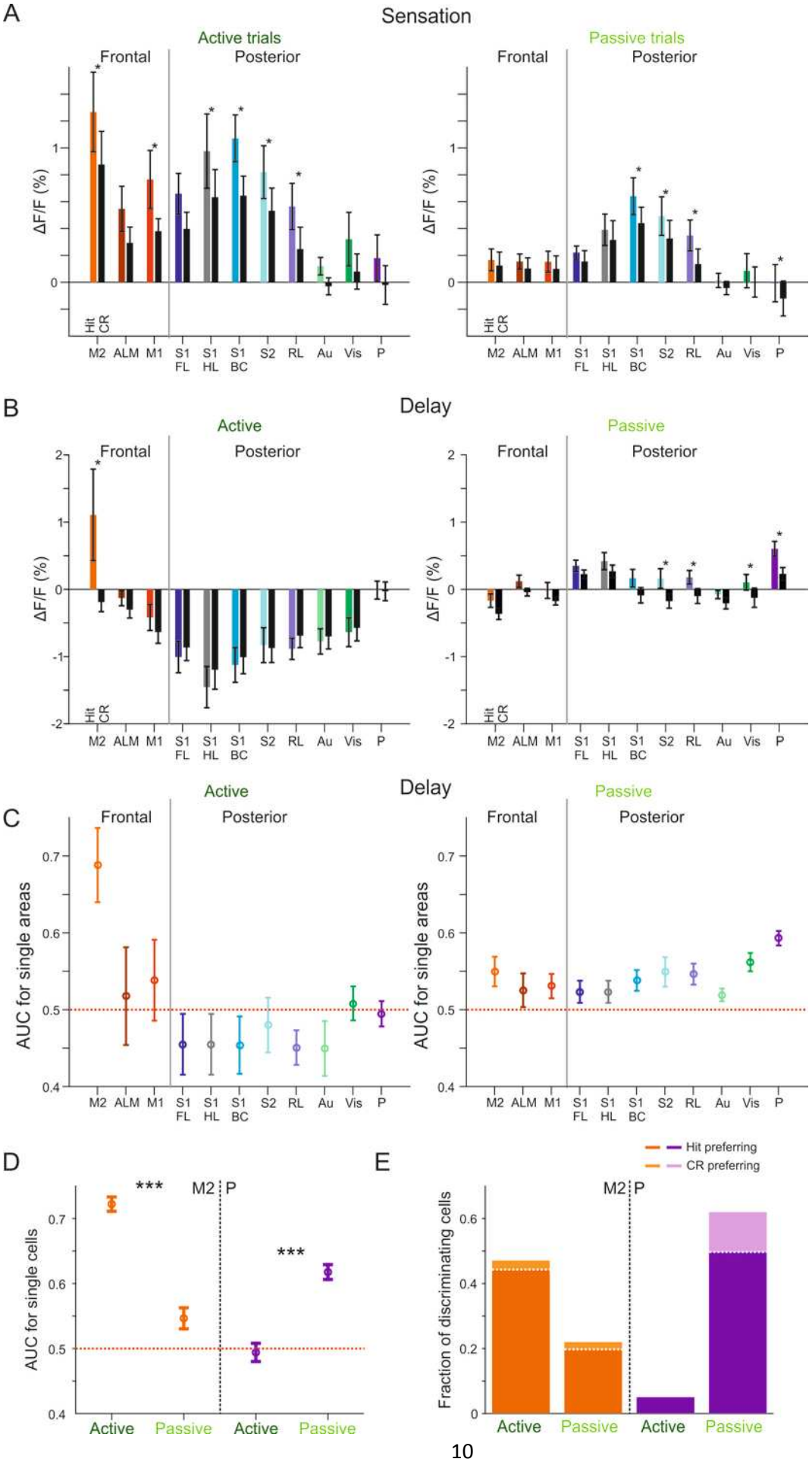
A
Sensation
Active trials
Passive trials
Frontal
Posterior
ΔF/F (%)
Hit
CR
M2 ALM M1 S1 FL S1 HL S1 BC S2 RL Au Vis P
B
Delay
Active
Passive
C
AUC for single areas
D
AUC for single cells
***
M2 | P
Active Passive Active Passive
E
Hit preferring
CR preferring
Fraction of discriminating cells

Figure S5. Related to Figures 2-5. Mean activity and decoding compared across all areas during the sensation and delay periods.

(A) Mean ΔF/F activity during the sensation period for all areas defined in this study and pooled across mice. Data are separated into active and passive trials and hit versus CR trials. Dashed line indicates separation between frontal and posterior cortex. Error bars are s.e.m across mice (n = 7 and 8 mice for active and passive trials, respectively). M2 – secondary motor cortex, ALM – anterior lateral motor cortex, M1 – primary motor cortex, S1FL – primary somatosensory forelimb cortex, S1HL – primary somatosensory hindlimb cortex, S1BC – primary somatosensory whisker cortex. S2 – secondary somatosensory whisker cortex. RL – posterior parietal cortex. Au – auditory cortex. Vis – visual cortex. P – posterior cortex. One-way ANOVA. * 95% confidence interval of response differences (hit minus CR) is different than zero.

(B) Same as in A but for the delay period. For the passive strategy S2, RL, and Vis show significant differences between hit and CR trials when pooling together all trials but differences were inconsistent within mice ($P > 0.05$ for 5 out of the 8 mice in S2, RL, and Vis; Wilcoxon signed-rank test across imaging sessions). One-way ANOVA. * 95% confidence interval of response differences (hit minus CR) is different than zero.

(C) Mean area under the ROC curve (AUC) for hit/CR discrimination during the delay period for single areas (left: active trials; right: passive trials). Error bar are s.e.m. across mice (n = 4 and 5 mice for active and passive strategies, respectively). This analysis is similar to the decoding in Figure 4, but here the decoder was applied to each area separately.

(D) Mean area under the ROC curve (AUC) for hit/CR discrimination during the delay period for individual L2/3 neurons in M2 (orange; n = 324 and 172 cells for active and passive trials, respectively) and in P (purple; n = 80 and 204 cells for active and passive trials, respectively). Only responsive neurons were included in the analysis (33% of all measured cells; STAR Methods). Error bars are S.E.M across cells. ***$P < 0.001$. Wilcoxon signed-rank test. Bonferroni corrected.

(E) Fraction of significantly discriminating L2/3 neurons in M2 (orange) and P (purple) in active or passive trials. Significance was assigned to a cell if its observed AUC value exceeded the 95% confidence limits derived from the sample distribution of trial-shuffled data (100 iterations). Cells preferring the hit trials (i.e., higher responses for hit vs. CR trials) are displayed as dark-shaded areas and cells preferring CR trials as light-shaded areas.

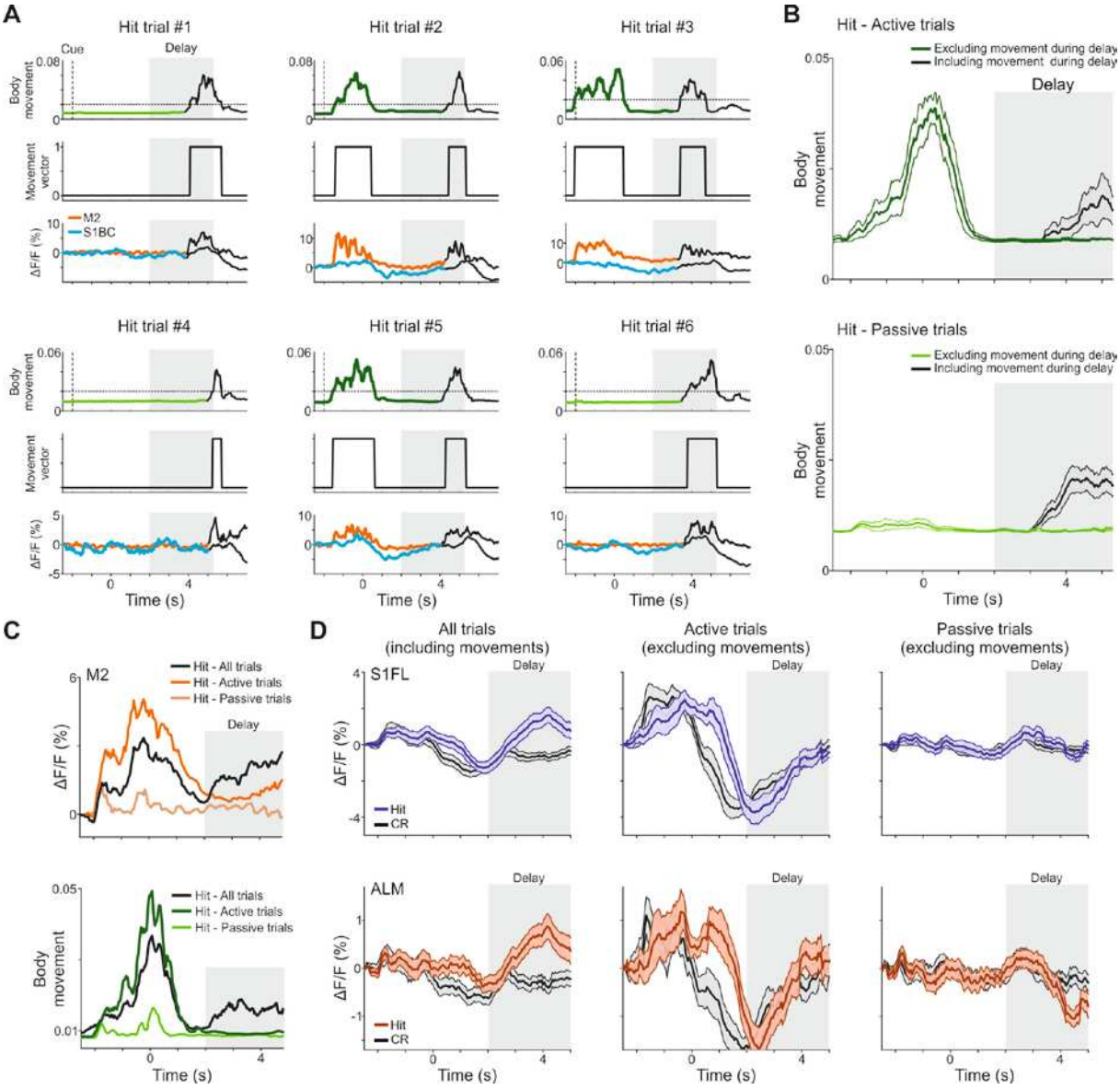

Figure S6. Related to Figure 3. Effects of movements on population responses and discarding movement periods during the delay period.

(A) Six example trials depicting the body movement (top; along with movement threshold in dashed line), the binary movement vector (middle; derived from taking a threshold on the body movement) and responses in the S1BC and M2 (bottom). Each trial was truncated just before the first move in the delay. Colored parts in each trial were taken for analysis excluding any movements during the delay and black parts were excluded from analysis. Active and passive trials are labeled in dark and light green respectively.

(B) Mean body movements in an example imaging session for active (top) and passive (bottom) hit trials only. In black are the same trials but without excluding movements in the delay. Error bar are s.e.m. across trials.

(C) An example recording session displaying responses in M2 (top) and body movements (bottom) for active (dark colors; excluding movement in the delay), passive (light colors; excluding movement in the delay), and all hit trials together (black; including movement in the delay). These movements

during the delay (not included in active and passive subgroups) correspond to an increase in M2 responses during the delay (black trace on top).

(D) Responses in hit and CR in S1FL (top) and ALM (bottom) for all (left; including movement in the delay), active (middle; excluding movement in the delay) and passive hit trials (right; excluding movement in the delay). Error bar are s.e.m. across trials. Movements during the delay correspond to an increase in ALM and S1FL responses during the delay.

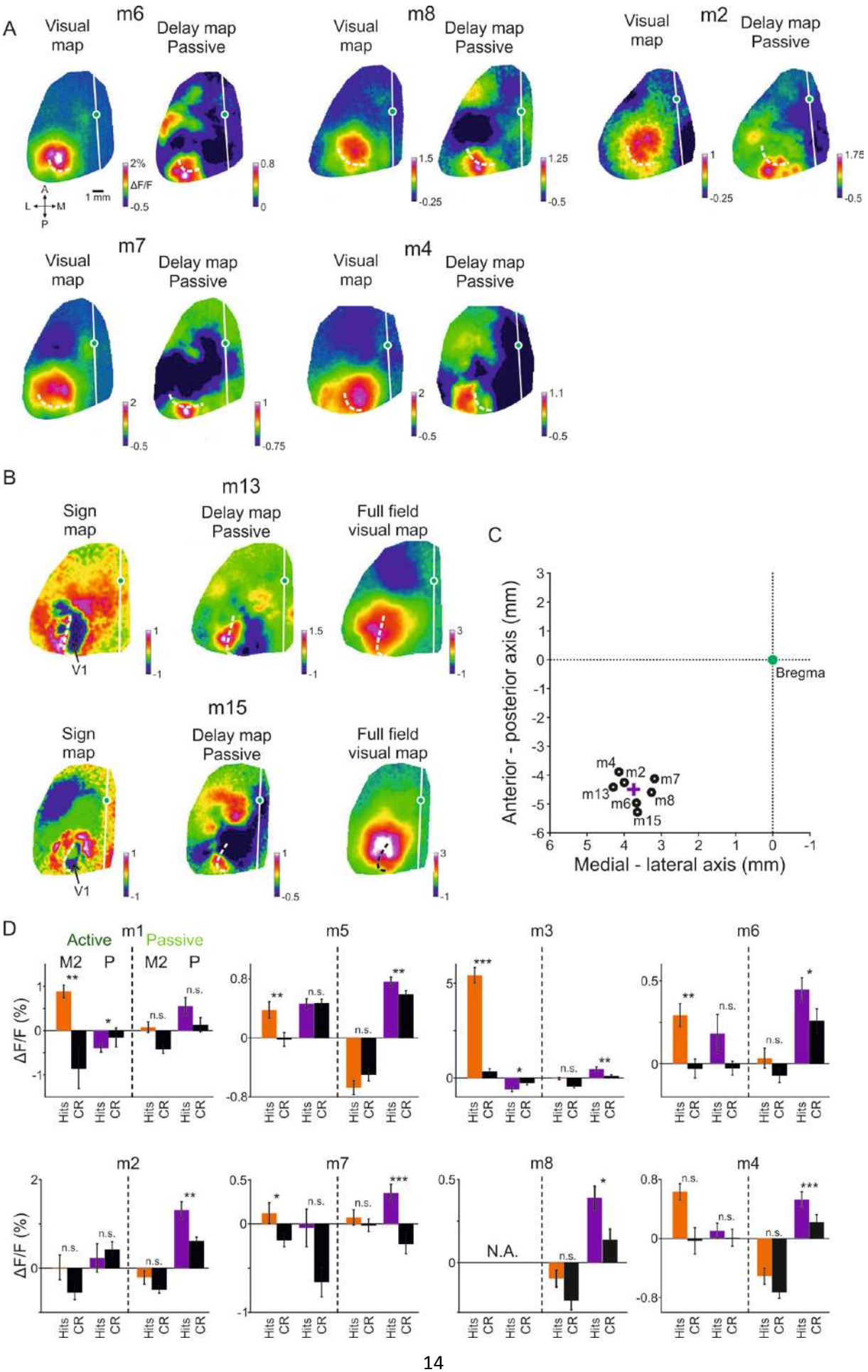
A
m6
Visual map
Delay map Passive
m8
m2
m7
m4
2%
ΔF/F
-0.5
1 mm
A
L
M
P
B
m13
Sign map
Delay map Passive
Full field visual map
V1
m15
C
Anterior - posterior axis (mm)
Medial - lateral axis (mm)
Bregma
m4
m2
m7
m13
m6
m8
m15
D
Active
Passive
m1
m5
m3
m6
m2
m7
m8
m4
ΔF/F (%)
M2
P
Hits
CR
N.A.
n.s.

Figure S7. Related to Figure3. Additional results and controls for the delay period.

(A-C) P area is localized posteriorly and laterally of the visual cortex.

(A) Comparison of a visual map and a delay map (registered together) for the 5 passive mice. *Left;* activation maps of a visual stimulation for each mouse (similar to Figure S2A). Dashed white line outlines the posterior and lateral boundary of the visual cortex. *Right:* Corresponding delay map for passive trials (as shown for passive mice in Figure 3B, D). Activation patches in all mice clearly are beyond the main activation of visual cortex (white dashed line).

(B) Comparison of a visual sign map (see STAR Methods), delay map and visual map (derived from a full field stimulus presented on a screen; all maps registered together) for 2 passive mice. Dashed white line outlines the posterior and lateral boundary of primary visual cortex (V1) derived from the sign map. Activation patches in both mice clearly lateral and posterior to V1 (white dashed line).

(C) Cortical coordinates (relative to bregma) for the center of the activation patch in the P area for each mouse (black circles) and the mean position (purple plus sign; 3.75 mm lateral and 4.51 mm posterior to bregma).

(D) Activations during the delay in M2 and P for each mouse (divided into active and passive trials; hit versus CR trials). Error bars are s.e.m. across imaging sessions. * $P < 0.05$. ** $P < 0.01$. *** $P < 0.001$. n.s. not significant. Wilcoxon signed-rank test.

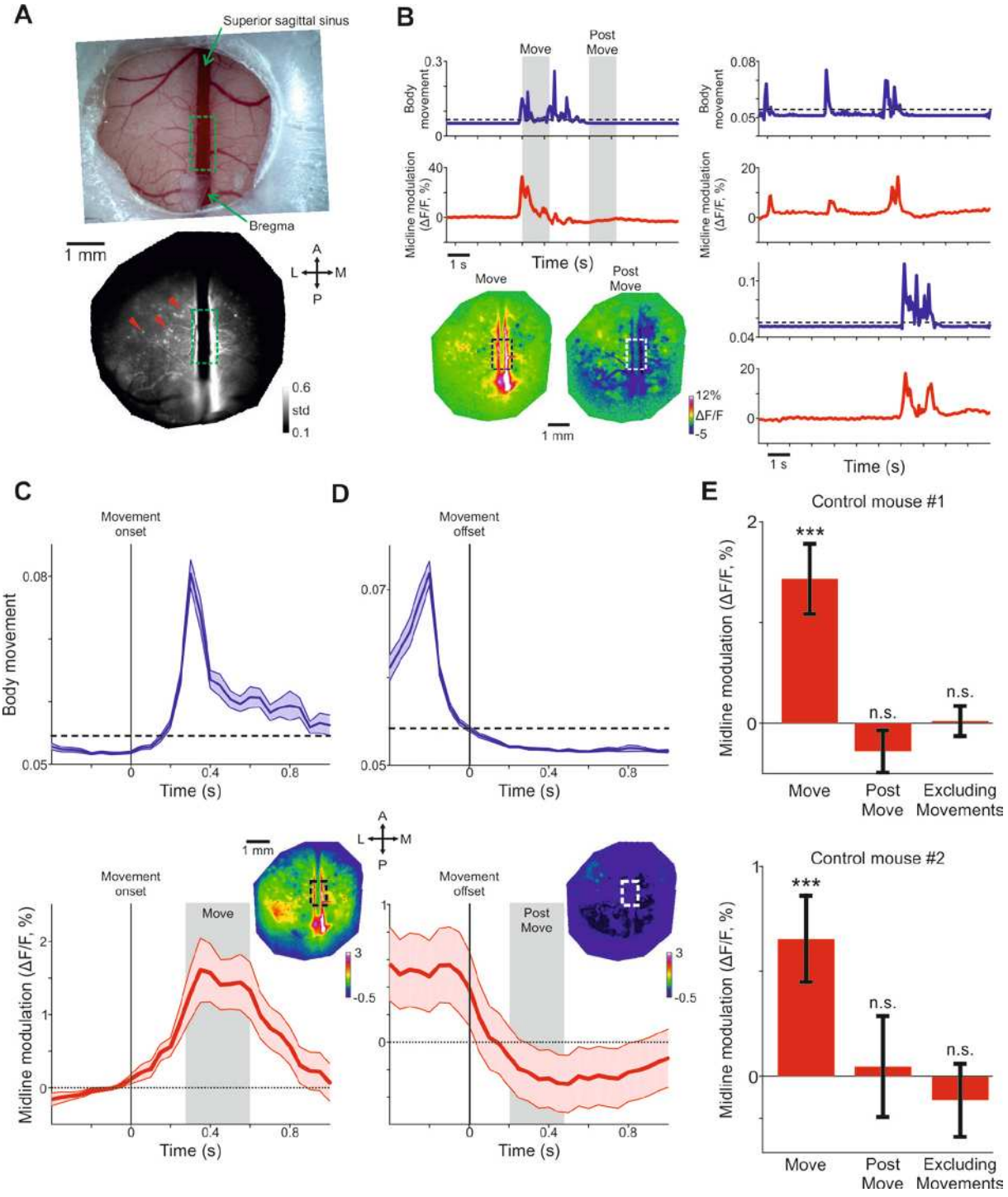

Figure S8. Related to Figure 3. Midline area is modulated during movement but returns to baseline shortly after.

(A) Two transgenic mice (expressing GCaMP6f in layer 2/3 excitatory cells) were implanted with a 5 mm glass window in the frontal cortex crossing the superior sagittal sinus (midline). *Bottom:* a map of standard deviation (over a 10 second trial of spontaneous activity) showing that midline area (green outline) displays high variance. Additional single cells are indicated in red arrows. Midline area close to M2 is outlined in green.

(B) Example trials during spontaneous activity showing body movement of the mouse (blue; top) and the midline modulation (red; bottom). Activation maps during movement and post movement periods are shown for one trial. Threshold for movement is in dashed black.

(C) Body movement (top) and midline modulation (bottom) triggered on movement onset. Corresponding activation map during movement (gray area in the middle) is showed in the inset. Error bars are s.e.m. across movement events (n=101).

(D) Same as C but triggered on movement offset. Activation map corresponds to 200-400 ms after movement offset.

(E) Mean midline modulation for movement, post-movement (200-400 ms after movement offset), and excluding all movements in two mice. Error bars are s.e.m. across movement events (n=101 and 112 movement event for mouse #1 and #2 respectively).

*** $P < 0.001$. n.s. not significant. Mann-Whitney U-test.

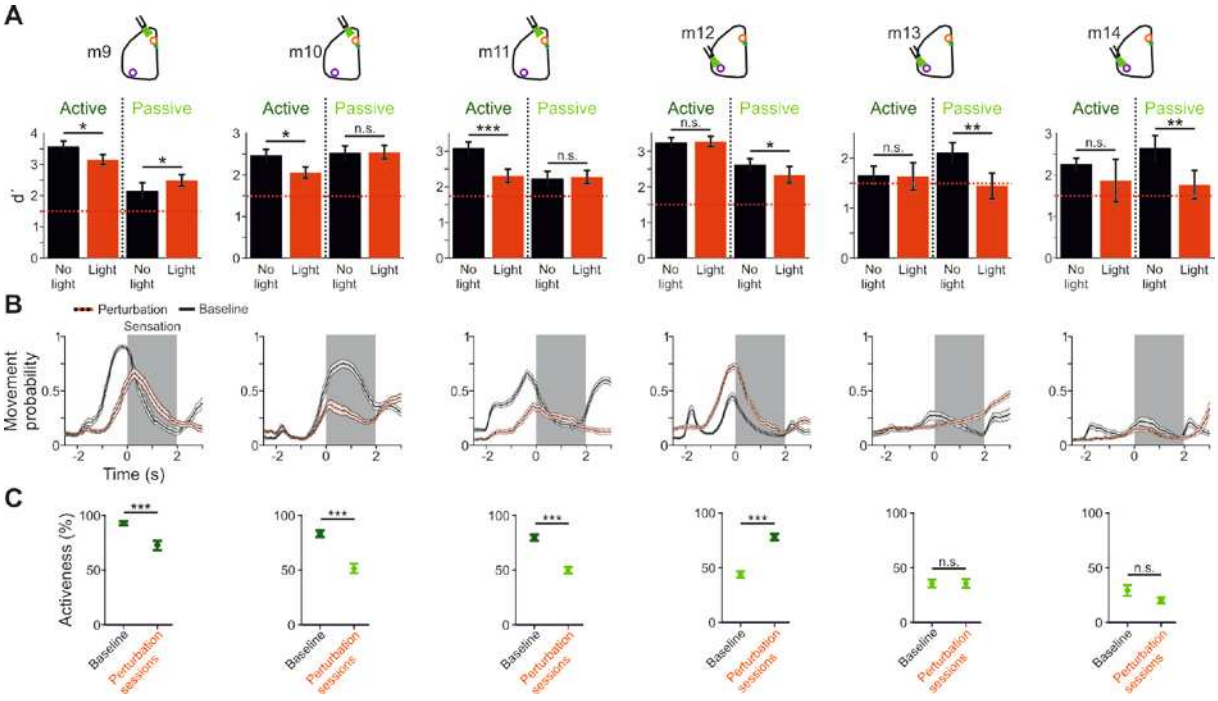

Figure S9. Related to Figure 6. Behavioral parameters for ArchT-mediated optogenetic experiments.

(A) Performance for all 6 mice (arranged from active to passive) used for the ArchT perturbations (mice 9-11 underwent M2 perturbation; mice 12-14 underwent P perturbation) during active and passive trial with and without light.

(B) Movement probability for the six mice during the perturbation sessions (black and red line; trials with and without light pooled together) and in baseline sessions (black line).

(C) Activeness for each mouse for perturbation and baseline sessions.

*P < 0.05, **P < 0.01, ***P < 0.001, n.s. not significant. Wilcoxon signed-rank test in a and Mann-Whitney U-test in B.

SUPPLEMENTARY VIDEOS

Video S1

Active hit trial in mouse #6. Related to Figure 3. *Top left:* Movie of the mouse body during the entire trial (body camera). Forelimb area is outlined in black. *Top right:* Movie of activity maps during the same trial. Color denotes normalized fluorescence (ΔF/F). M2 and P areas are outlined in red and blue respectively. *Bottom:* Traces of M2 (red) and P (blue) areas, forelimb movements (dashed black), whisker envelope (black) and licking detector (thin red). Sensation and delay periods are marked in light blue and green respectively.

Video S2

Passive hit trial in mouse #6. Related to Figure 3. *Top left:* Movie of the mouse body during the entire trial (body camera). Forelimb area is outlined in black. *Top right:* Movie of activity maps during the same trial. Color denotes normalized fluorescence (ΔF/F). M2 and P areas are outlined in red and blue respectively. *Bottom:* Traces of M2 (red) and P (blue) areas, forelimb movements (dashed black), whisker envelope (black) and licking detector (thin red). Sensation and delay periods are marked in light blue and green respectively.

Video S3

Active hit trial in mouse #5. Related to Figure 3. *Top left:* Movie of the mouse body during the entire trial (body camera). Forelimb area is outlined in black. *Top right:* Movie of activity maps during the same trial. Color denotes normalized fluorescence (ΔF/F). M2 and P areas are outlined in red and blue respectively. *Bottom:* Traces of M2 (red) and P (blue) areas, forelimb movements (dashed black), whisker envelope (black) and licking detector (thin red). Sensation and delay periods are marked in light blue and green respectively.

Video S4

Passive hit trial in mouse #7. Related to Figure 3. *Top left:* Movie of the mouse body during the entire trial (body camera). Forelimb area is outlined in black. *Top right:* Movie of activity maps during the same trial. Color denotes normalized fluorescence (ΔF/F). M2 and P areas are outlined in red and blue respectively. *Bottom:* Traces of M2 (red) and P (blue) areas, forelimb movements (dashed black), whisker envelope (black) and licking detector (thin red). Sensation and delay periods are marked in light blue and green respectively.